Journal of the Mechanics and Physics of Solids 143 (2020) 104040

Contents lists available at ScienceDirect

Journal of the Mechanics and Physics of Solids

journal homepage: www.elsevier.com/locate/jmps

A new approach to the mechanics of DNA: Atoms-to-beam homogenization

Johannes Kalliauer[a], Gerhard Kahl[b], Stefan Scheiner[a], Christian Hellmich[a,*]

[a] Institute for Mechanics of Materials and Structures, TU Wien – Vienna University of Technology, Karlsplatz 13/202, 1040 Vienna, Austria
[b] Institute for Theoretical Physics, TU Wien – Vienna University of Technology, Wiedner Hauptstraße 8-10/136, 1040 Vienna, Austria

ARTICLE INFO

Article history:
Received 2 April 2020
Accepted 24 May 2020
Available online xxx

Keywords:
Linear elasticity
Beam
Energy methods
Finite differences
Flexibility
Young's modulus
Stretching stiffness
Free energy

ABSTRACT

It is useful to describe the deformation characteristics of long biological macromolecules, such as deoxyribonucleic acid (DNA), by means of terms such as "bending", "stretching", or "twisting". These terms are borrowed from classical beam theory, a traditional and widely known subfield of continuum mechanics, whereas the standard numerical modeling procedure for macromolecules, which is molecular dynamics, does not allow for explicit introduction of the aforementioned deformation modes. This somehow puts some limit to the mechanical understanding of biological macromolecules. As a remedy, we here propose an upscaling (or homogenization) approach, spanning a new conceptual bridge from molecular dynamics to beam theory. Firstly, we apply the principle of virtual power (PVP) to classical continuum beams subjected to stretching and twisting, as well as to atomic compounds represented as discrete systems of mass points in the framework of molecular dynamics. Equating virtual power densities associated with continuum and discrete representations provides homogenization rules from the atomic compounds to the continuum beam line elements. Secondly, the forces acting on the aforementioned mass points are derived from energy potentials associated with bond stretching, valence and torsion angle variations, as well as electrostatic and van der Waals interactions. Application of this strategy to a specific DNA sequence consisting of 20 base pairs reveals deformation-dependent conformational changes, as well as paradox phenomena such as "stretching due to overwinding", in line with known experimental observations.

1. Introduction

For several decades, substantial experimental, theoretical, and computational efforts have been undertaken to decipher the mechanical properties of double-stranded DNA (i.e. deoxyribonucleic acid). At the so-called flexural persistence length of around 50 nm and below (Baumann et al., 1997; Bustamante et al., 2003; Herrero-Galán et al., 2013), DNA appears as elastic rod undergoing stretching, bending, and twisting. In contrast, very long DNA strands, up to lengths of tens of micrometers and beyond (Bustamante et al., 2000), behave more like ropes which can take a variety of different conformational states (Bauer et al., 1993; Benham and Mielke, 2005; Boles et al., 1990; Herrero-Galán et al., 2013). Notably, these conformational

* Corresponding author.
E-mail address: christian.hellmich@tuwien.ac.at (C. Hellmich).

https://doi.org/10.1016/j.jmps.2020.104040

states are associated with important biological processes such as replication, folding, packaging, regulation, recombination, and gene expression, including transcription and translation (Bustamante et al., 2003; Naserian-Nik et al., 2013; Olson et al., 1993).

On the experimental side, translational motions of magnetic beads attached to the ends of single- and double-stranded DNA molecules allowed for controlled uncoiling of the DNA threads, and for recording of respective force-extension relations. In combination with extensible worm-like chain models, the aforementioned force-extension relations give access to an elastic stretch modulus of the molecule of around 1 nN, identified for a loading state characterized by an axial force of around 10 pN (Baumann et al., 1997; Bustamante et al., 2000; Herrero-Galán et al., 2013; Smith et al., 1992). Rotational movement of magnetic beads, in combination with classical torsional beam theory (Barkley and Zimm, 1979) allowed for quantification of the torsional stiffness of DNA of around 400 pN nm^2 (Bryant et al., 2003). However, classical beam theory ignores characteristic features of DNA rods and ropes, such as the strong coupling between stretching, torsion, and bending (Gore et al., 2006; Gross et al., 2011; Lionnet et al., 2006). This coupling stems from the complex atomic structure of DNA, which can be modeled in much more detail by means of molecular dynamics simulations (Cluzel et al., 1996; Galindo-Murillo et al., 2015; Grindon et al., 2004; Kosikov et al., 1999; Lavery et al., 2002, 2010; Mathew-Fenn et al., 2008; Orozco et al., 2008; Šponer et al., 2006). However, the results of such simulations (i.e., displacements and the potentials of the involved atoms) have been rarely (if at all) linked to the classical notions of stretching, bending, and torsional stiffnesses, as introduced in beam mechanics.

It is the establishment of such a link between the atom-wise behavior of DNA upon mechanical loading and the corresponding stiffnesses, which is the key contribution of the present paper. For this purpose, the principle of virtual power (PVP) (Germain, 1973; Touratier, 1991) is applied to both classical beam theory and to discrete force systems (Salenccon and Lyle, 2001) representing atomic compounds in molecular dynamics simulations. In this way, we utilize the PVP as a theoretical vehicle for "homogenizing" the beam-like atomistic compounds into continuum beams with coupled stretching-torsion characteristics. Accordingly, this paper is organized as follows: First, atom-to-beam homogenization rules are derived from the PVP, providing upscaling relations between the forces acting on the atoms on the one hand, and the DNA-beam-element-specific normal forces and torsional moments, on the other hand (see Section 2). Thereafter, the aforementioned atom-related forces are derived from energy potentials associated with the stretching of covalent bonds, the bending of angles between covalent bonds, and torsion of covalent bonds (see Section 3), as well as from van der Waals and electrostatic interactions (see Section 4). The resulting atomic forces and energies are presented in Section 5. Numerical solution procedures for DNA rods made of 10 to 60 adeninethymine base pairs, subjected to different stretching and torsional deformations, are described in Section 6, followed by the presentation of the gained results (in Section 7), and of the respective conclusions (in Section 8).

2. Twisting and stretching of continuous rods and of rod-like atomic compounds

2.1. Principle of virtual power applied to continuous rods

The principle of virtual power (PVP) allows for an elegant development of the continuum mechanical representation of twisting and stretching rods. Paraphrasing from (Germain, 1973; Salenccon and Lyle, 2001), the underlying principle can be summarized as follows: *"Let a system S [of forces in a general sense] fulfill the fundamental law of dynamics with respect to a given Galilean frame; then, in any virtual motion, the sum of the virtual powers of the internal forces and of the external forces are equal to the virtual power of the acceleration forces."*

In a straight beam subjected to stretching and twisting, the virtual motion is fully described through continuous distributions of the axial virtual velocity $\hat{v}$ and the axial virtual angular velocity $\hat{\Omega}$ along the beam axis; with positions along this axis being labeled by coordinate X (i.e., the *macroscopic* location quantity). The virtual power of internal forces is governed by velocity gradients (Germain, 1973; Salenccon and Lyle, 2001; Touratier, 1991); hence, the expression for straight beams undergoing stretching and twisting reads as (Kuttke et al., 2019)

$$\mathcal{P}_{\text{int}}^{\text{cont}} = \int_{X=0}^{X=L} \left(-N(X)\, \frac{\partial \hat{V}(X)}{\partial X} - M_x(X)\, \frac{\partial \hat{\Omega}(X)}{\partial X} \right) \mathrm{d}X \,, \tag{1}$$

where L is the length of the beam, N is the axial (or normal) force, and M_x is the axial (or torsional) moment. On the other hand, the virtual power of external forces is associated with the velocity quantities themselves, so that

$$\mathcal{P}_{\text{ext}}^{\text{cont}} = \left[N(X)\, \hat{V}(X) + M_x(X)\, \hat{\Omega}(X) \right]_{X=0}^{X=L} + \int_{X=0}^{X=L} \left(n_x(X)\, \hat{V}(X) + m_x(X)\, \hat{\Omega}(X) \right) \mathrm{d}X \,, \tag{2}$$

with n_x and m_x as the axial line load and the torsional moment per length, respectively. Finally, in the equilibrium (or static) case of negligibly small accelerations, the PVP mathematically reads as

$$\mathcal{P}_{\text{ext}}^{\text{cont}} + \mathcal{P}_{\text{int}}^{\text{cont}} = 0 \,, \tag{3}$$

with $\mathcal{P}_{\text{int}}^{\text{cont}}$ and $\mathcal{P}_{\text{ext}}^{\text{cont}}$ defined in Eqs. (1) and (2). The integrands in Eqs. (1) and (2) are virtual power densities (of dimensions power per unit length), and they may be explicitly given as

$$\wp_{\text{int}}^{\text{cont}}(X) = -N(X)\, \frac{\partial \hat{V}(X)}{\partial X} - M_x(X)\, \frac{\partial \hat{\Omega}(X)}{\partial X} \,, \tag{4}$$

and

$$\mathcal{P}_{\text{ext}}^{\text{cont}}(X) = n_x(X)\,\hat{V}(X) + m_x(X)\,\hat{\Omega}(X)\,. \tag{5}$$

2.2. Principle of virtual power applied to rod-like atomic compounds

Next, we consider an atomic compound which resolves a continuum line element dX of DNA into *microstructural* details. The line element dX exhibits an actual physical length ℓ_{RLE}, with RLE standing for *representative line element*, in analogy to the *representative volume element* in continuum (material) micromechanics (Zaoui, 2002). At the *microstructural* level, the line element appears as a volume hosting a set of mass points, whereby each of them represents one atom. Microstructural positions within this volume are labeled by location vector $\mathbf{x} = x\,\mathbf{e}_x + y\,\mathbf{e}_y + z\,\mathbf{e}_z$, whereby base vector $\mathbf{e}_x$ points in the longitudinal direction of the straight beam, and base vectors $\mathbf{e}_y$ and $\mathbf{e}_z$ span the cross sections of the beam. In a molecular dynamics (MD) setting, the force acting on atom i, considering thereby a conservative force field, is identical to the negative gradient of the potential energy E_{pot} (Allen, 2004; Arnol'd et al., 2013; Srivastava, 1997),

$$\mathbf{F}_i = -\boldsymbol{\nabla}_i E_{\text{pot}} = -\frac{\mathrm{d}E_{\text{pot}}}{\mathrm{d}\mathbf{x}_i}\,. \tag{6}$$

Hereby, the potential E_{pot} is the sum of energy contributions stemming from covalent bonds subjected to stretching, bending, and torsion (see Section 3 for further details); from van der Waals forces (see Section 4 for further details); and from electrostatic interactions (see also Section 4 for further details). The forces appearing in Eq. (6) are then assigned to one of the following two categories:

- If all the atoms associated with a bonding, a non-bonding, or an electrostatic interaction are located *within* the microscopic volume associated with line element dX, then the corresponding forces are called internal forces, and their sum in position $\mathbf{x}_i$ results in the internal force of mass point i, called $\mathbf{F}_i^{\text{int}}$, $\mathbf{F}_i^{\text{int}} = F_{i,x}^{\text{int}}\,\mathbf{e}_x + F_{i,y}^{\text{int}}\,\mathbf{e}_y + F_{i,z}^{\text{int}}\,\mathbf{e}_z$.
- If one or more of the atoms associated with a bonding, a non-bonding, or an electrostatic interaction are located *outside* the microscopic volume associated with line element dX, the remaining members of the bonding, the non-bonding, or the electrostatic interactions are subjected to external forces, and the sum of these forces in position $\mathbf{x}_i$ results in the external force of mass point i, called $\mathbf{F}_i^{\text{ext}}$, $\mathbf{F}_i^{\text{ext}} = F_{i,x}^{\text{ext}}\,\mathbf{e}_x + F_{i,y}^{\text{ext}}\,\mathbf{e}_y + F_{i,z}^{\text{ext}}\,\mathbf{e}_z$.

The virtual power densities associated with these internal and external forces read as

$$\mathcal{P}_{\text{int}}^{\text{atom}} = \frac{1}{\ell_{\text{RLE}}}\sum_{i=1}^{N_{\text{atom}}} \mathbf{F}_i^{\text{int}}(\mathbf{x}_i)\cdot\hat{\mathbf{v}}^{\text{int}}(\mathbf{x}_i)\,, \tag{7}$$

and

$$\mathcal{P}_{\text{ext}}^{\text{atom}} = \frac{1}{\ell_{\text{RLE}}}\sum_{i=1}^{N_{\text{atom}}} \mathbf{F}_i^{\text{ext}}(\mathbf{x}_i)\cdot\hat{\mathbf{v}}^{\text{ext}}(\mathbf{x}_i)\,, \tag{8}$$

with $\mathbf{x}_i = x_i\,\mathbf{e}_x + y_i\,\mathbf{e}_y + z_i\,\mathbf{e}_z$ as the microscopic location vector of atom i, and with N_{atom} being the number of atoms of the RLE. The microscopic virtual velocity fields $\hat{\mathbf{v}}^{\text{int}}$ and $\hat{\mathbf{v}}^{\text{ext}}$ are associated to the continuum beam kinematics defined in Section 2.1, via axial translations $\hat{V}$ and axial rotations $\hat{\Omega}$ of rigid cross sections:

- According to Eq. (1), the internal forces are linked to macroscopic virtual velocity gradients. The simplest form of a corresponding microscopic virtual field reads as

$$\hat{\mathbf{v}}^{\text{int}}(\mathbf{x}_i) = x_i\left(\frac{\partial\hat{V}(X)}{\partial X}\,\mathbf{e}_x + \frac{\partial\hat{\Omega}(X)}{\partial X}\,(-z_i\,\mathbf{e}_y + y_i\,\mathbf{e}_z)\right). \tag{9}$$

- According to Eq. (2), the external forces are linked to the macroscopic virtual velocities themselves. The simplest form of a corresponding microscopic virtual field reads as

$$\hat{\mathbf{v}}^{\text{ext}}(\mathbf{x}_i) = \hat{V}(X)\,\mathbf{e}_x + \hat{\Omega}(X)\,(-z_i\,\mathbf{e}_y + y_i\,\mathbf{e}_z)\,. \tag{10}$$

Insertion of Eq. (9) into Eq. (7), and of Eq. (10) into Eq. (8) yields the atom-related virtual power densities as

$$\mathcal{P}_{\text{int}}^{\text{atom}} = \frac{1}{\ell_{\text{RLE}}}\sum_{i=1}^{N_{\text{atom}}} \mathbf{F}_i^{\text{int}}(\mathbf{x}_i)\cdot\left(\frac{\partial\hat{V}(X)}{\partial X}\,\mathbf{e}_x + \frac{\partial\hat{\Omega}(X)}{\partial X}\,(-z_i\,\mathbf{e}_y + y_i\,\mathbf{e}_z)\right)x_i\,, \tag{11}$$

and

$$\mathcal{P}_{\text{ext}}^{\text{atom}} = \frac{1}{\ell_{\text{RLE}}}\sum_{i=1}^{N_{\text{atom}}} \mathbf{F}_i^{\text{ext}}(\mathbf{x}_i)\cdot\left(\hat{V}(X)\,\mathbf{e}_x + \hat{\Omega}(X)\,(-z_i\,\mathbf{e}_y + y_i\,\mathbf{e}_z)\right). \tag{12}$$

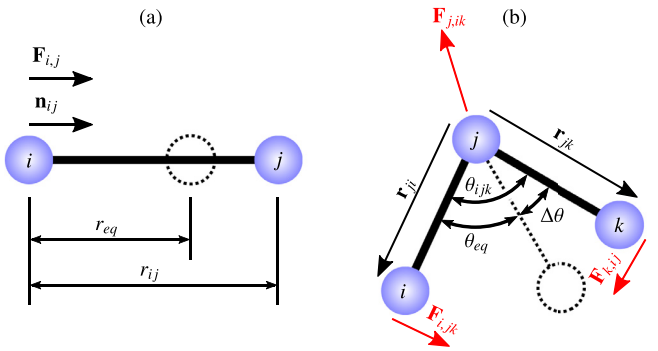

Fig. 1. Deformations of covalent bonds between atoms, including (a) stretching, and (b) bending; the cartoon was inspired by (Ilse, 2016; Lengvarsky and Bocko, 2015).

2.3. Homogenization rules derived from the principle of virtual power

Setting $\mathcal{P}_{\text{int}}^{\text{cont}}$ according to Eq. (4) equal to $\mathcal{P}_{\text{int}}^{\text{atom}}$ according to Eq. (11), as well as $\mathcal{P}_{\text{ext}}^{\text{cont}}$ according to Eq. (5) equal to $\mathcal{P}_{\text{ext}}^{\text{atom}}$ according to Eq. (12), and requiring these identities to hold for any virtual motions $\hat{V}(X), \partial\hat{V}/\partial X, \hat{\Omega}(X), \partial\hat{\Omega}/\partial X$, yields the following atoms-to-beam homogenization (or averaging) rules:

$$N(X) = -\frac{1}{\ell_{\text{RLE}}} \sum_{i=1}^{N_{\text{atom}}} x_i \, F_{i,x}^{\text{int}} \,, \tag{13}$$

$$M_x(X) = -\frac{1}{\ell_{\text{RLE}}} \sum_{i=1}^{N_{\text{atom}}} x_i \left(-z \, F_{i,y}^{\text{int}} + y \, F_{i,z}^{\text{int}}\right), \tag{14}$$

$$n_x(X) = \frac{1}{\ell_{\text{RLE}}} \sum_{i=1}^{N_{\text{atom}}} F_{i,x}^{\text{ext}} \,, \tag{15}$$

and

$$m_x(X) = \frac{1}{\ell_{\text{RLE}}} \sum_{i=1}^{N_{\text{atom}}} \left(-z \, F_{i,y}^{\text{ext}} + y \, F_{i,z}^{\text{ext}}\right). \tag{16}$$

3. Covalent bonding-related potentials and forces

3.1. Stretching of covalent bonds

The potential energy associated with the stretching of a covalent bond between two atoms with positions $\mathbf{x}_i$ and $\mathbf{x}_j$ is given through (Boyd, 1968; Ivani, 2016)

$$\tilde{E}_{\text{bond}}^{ij} = k_{ij} \left(r_{ij} - r_{\text{eq}}\right)^2 = k_{ij} \left(\Delta r\right)^2 , \tag{17}$$

with the bond term constant k_{ij}, the equilibrium distance r_{eq}, and the actual distance measure r_{ij}, defined through

$$r_{ij} = \|\mathbf{r}_{ij}\| = \|\mathbf{x}_j - \mathbf{x}_i\| \,. \tag{18}$$

The force acting on atom i with position $\mathbf{x}_i$, stemming from a covalent bond between atoms i and j reads as (Monasse and Boussinot, 2014)

$$\tilde{\mathbf{F}}_{\text{bond}}^{i,j} = -\frac{\mathrm{d}\tilde{E}_{\text{bond}}^{ij}}{\mathrm{d}\mathbf{x}_i} = 2\, k_{ij} \, \Delta r \, \frac{\mathbf{x}_j - \mathbf{x}_i}{\|\mathbf{x}_j - \mathbf{x}_i\|} = 2\, k_{ij} \, \Delta r \, \mathbf{n}_{ij} \,, \tag{19}$$

with $\mathbf{n}_{ij}$ as the unit vector pointing from atom i to atom j, see Fig. 1(a).

3.2. Bending of angle between two connected covalent bonds

The potential associated with a changing angle between two covalent bonds, formed between atoms i and j and atoms j and k (also referred as bending of the angle), is given through (Allen and Tildesley, 2017; Boyd, 1968)

$$\tilde{E}_{\text{angle}}^{ijk} = k_{ijk} \left(\theta_{ijk} - \theta_{\text{eq}}\right)^2 = k_{ijk} \left(\Delta\theta\right)^2 , \tag{20}$$

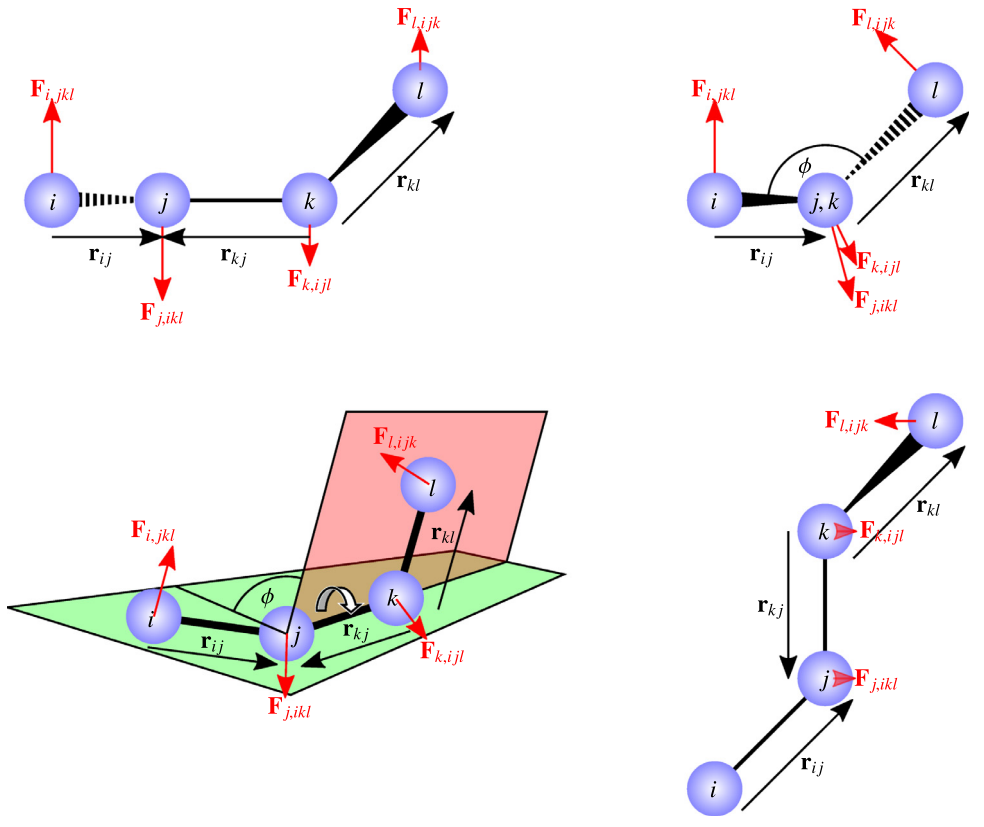

Fig. 2. Deformations related to changing dihedral angles, showing in particular proper torsion of covalent bonds; the cartoon was inspired by (Allen and Tildesley, 2017; Boussinot and Monasse, 2013; Case, 2019). The bonds in the first-angle projection are illustrated using the standard wedge-dash notation (Burrmann and Moore, 2013).

with the angle force constant k_{ijk}, the equilibrium angle θ_{eq}, and the valence angle θ_{ijk} between three atoms i, j and k, defined through $\theta_{ijk} = \arccos(\mathbf{n}_{ji} \cdot \mathbf{n}_{jk})$.

The force acting on atom i, with position $\mathbf{x}_i$, stemming from a bending potential associated with atoms i, j and k, and with the angle positioned at atom j, see Fig. 1(b), reads as (Allen and Tildesley, 2017; Monasse and Boussinot, 2014)

$$\tilde{\mathbf{F}}^{i,jk}_{\text{angle}} = -\frac{\mathrm{d}\tilde{E}^{ijk}_{\text{angle}}}{\mathrm{d}\mathbf{x}_i} = -\left(2\,k_{ijk}\,\Delta\theta\,\frac{\partial\theta[\mathbf{n}_{ji}(\mathbf{x}_i)]}{\partial\mathbf{x}_i}\right) = -\frac{2\,k_{ijk}\,\Delta\theta\,\mathbf{r}_{ji}\times\left(\mathbf{r}_{ji}\times\mathbf{r}_{jk}\right)}{r_{ij}\left\|\mathbf{r}_{ji}\times\left(\mathbf{r}_{ji}\times\mathbf{r}_{jk}\right)\right\|}\,. \tag{21}$$

On the other hand, the force acting on atom k, with position $\mathbf{x}_k$, stemming from a bending potential associated with atoms i, j and k, is defined analogously, reading as (Allen and Tildesley, 2017; Monasse and Boussinot, 2014)

$$\tilde{\mathbf{F}}^{k,ij}_{\text{angle}} = -\frac{\mathrm{d}\tilde{E}^{ijk}_{\text{angle}}}{\mathrm{d}\mathbf{x}_k} = -\frac{2\,k_{ijk}\,\Delta\theta\,\mathbf{r}_{kj}\times\left(\mathbf{r}_{ji}\times\mathbf{r}_{jk}\right)}{r_{jk}\left\|\mathbf{r}_{kj}\times\left(\mathbf{r}_{ji}\times\mathbf{r}_{jk}\right)\right\|}\,. \tag{22}$$

Finally, the force acting on atom j, with position $\mathbf{x}_j$, stemming from a bending potential associated with atoms i, j and k, follows from straightforward equilibrium considerations and reads as (Monasse and Boussinot, 2014)

$$\tilde{\mathbf{F}}^{j,ik}_{\text{angle}} = -\tilde{\mathbf{F}}^{i,jk}_{\text{angle}} - \tilde{\mathbf{F}}^{k,ij}_{\text{angle}}. \tag{23}$$

Additionally, it should be noted that Eqs. (21)–(23) ensure moment equilibrium of all forces related to this specific potential (Monasse and Boussinot, 2014),

$$\tilde{\mathbf{M}} = \mathbf{x}_i \times \tilde{\mathbf{F}}^{i,jk}_{\text{angle}} + \mathbf{x}_k \times \tilde{\mathbf{F}}^{k,ij}_{\text{angle}} + \mathbf{x}_j \times \tilde{\mathbf{F}}^{j,ik}_{\text{angle}} = 0\,. \tag{24}$$

3.3. Torsion of covalent bonds

The potential associated with a changing dihedral angle between two planes, each spanned by three atoms (see Fig. 2), reads as (Pearlman et al., 1995; Pérez et al., 2007)

$$\tilde{E}^{ijkl}_{\text{dihedral}} = k_{ijkl}\left[1 + \cos(n\,\phi)\,\cos(\psi) + \sin(n\,\phi)\,\sin(\psi)\right]\eta\,, \tag{25}$$

with the torsional constant k_{ijkl}, the periodicity n, the phase angle ψ, the torsional (dihedral) angle ϕ, and the variable η, being either $\eta = 0$ if the dihedral is (almost) linear or $\eta = 1$ otherwise. Thereby, both or either of the following two criteria must be fulfilled for considering a dihedral angle as linear: $(\|\mathbf{n}_{ij} \times \mathbf{n}_{kl}\| < 10^{-3})$ and $(\|\mathbf{n}_{kl} \times \mathbf{n}_{kj}\| < 10^{-3})$. Furthermore, if $\eta = 1$, ϕ is defined through (Case, 2019)

$$\phi = \pi - \text{sign}\left(\arccos\left(\frac{(\mathbf{r}_{ij} \times \mathbf{r}_{kj}) \cdot (\mathbf{r}_{kl} \times \mathbf{r}_{kj})}{\|\mathbf{r}_{ij} \times \mathbf{r}_{kj}\| \, \|\mathbf{r}_{kl} \times \mathbf{r}_{kj}\|}\right), \mathbf{r}_{kj} \cdot \left((\mathbf{r}_{kl} \times \mathbf{r}_{kj}) \times (\mathbf{r}_{ij} \times \mathbf{r}_{kj})\right)\right), \tag{26}$$

making use of the following definition: $\text{sign}(A, B) = \text{abs}(A)$ if $B \geq 0$, and $\text{sign}(A, B) = -\text{abs}(A)$ otherwise. Notably, Eq. (25) holds for both proper torsion (as depicted in Fig. 2) and improper torsion. The latter represents the case that one central atom is bonded to all three other atoms, while those four atoms still form a dihedral angle (Case, 2019). The occurrence of proper and improper torsion depends on the considered force field as well as the studied atoms.

The force acting on atom i, with position $\mathbf{x}_i$, stemming from a dihedral potential between atoms i, j, k and l, reads as

$$\tilde{\mathbf{F}}^{i,jkl}_{\text{dihedral}} = \frac{k_{ijkl}\, n\, \sin(n\,\phi - \psi)\, \mathbf{r}_{ji} \times \mathbf{r}_{jk}}{r_{ij}\, \|\mathbf{r}_{ji} \times \mathbf{r}_{jk}\| \sin\left(\arccos\left(\frac{\mathbf{r}_{ji} \cdot \mathbf{r}_{jk}}{r_{ij}\, r_{jk}}\right)\right)}. \tag{27}$$

On the other hand, the force acting on atom l, with position $\mathbf{x}_l$, stemming from a dihedral potential associated with atoms i, j, k and l, is defined analogously, reading as

$$\tilde{\mathbf{F}}^{l,ijk}_{\text{dihedral}} = \frac{k_{ijkl}\, n\, \sin(n\,\phi - \psi)\, \mathbf{r}_{kl} \times \mathbf{r}_{kj}}{r_{kl}\, \|\mathbf{r}_{kl} \times \mathbf{r}_{kj}\| \sin\left(\arccos\left(\frac{\mathbf{r}_{kj} \cdot \mathbf{r}_{kl}}{r_{jk}\, r_{kl}}\right)\right)}, \tag{28}$$

whereas the force acting on atom k, with position $\mathbf{x}_k$, stemming from a dihedral potential associated with atoms i, j, k and l, reads as (Monasse and Boussinot, 2014)

$$\tilde{\mathbf{F}}^{k,ijl}_{\text{dihedral}} = \frac{1}{r_{jk}^2}\left(-\mathbf{r}_{jk} \times \tilde{\mathbf{F}}^{l,ijk}_{\text{dihedral}} + \mathbf{r}_{kl} \times \tilde{\mathbf{F}}^{l,ijk}_{\text{dihedral}} + \mathbf{r}_{ji} \times \tilde{\mathbf{F}}^{i,jkl}_{\text{dihedral}}\right) \times \mathbf{r}_{jk}. \tag{29}$$

Finally, the force acting on atom j, with position $\mathbf{x}_j$, stemming from a dihedral potential associated with atoms i, j, k and l, follows again from equilibrium considerations, and reads as (Monasse and Boussinot, 2014)

$$\tilde{\mathbf{F}}^{j,ikl}_{\text{dihedral}} = -\tilde{\mathbf{F}}^{i,jkl}_{\text{dihedral}} - \tilde{\mathbf{F}}^{l,ijk}_{\text{dihedral}} - \tilde{\mathbf{F}}^{k,ijl}_{\text{dihedral}}. \tag{30}$$

Analogously to the bending potential presented in Section 3.2, Eqs. (27) – (30) ensure moment equilibrium of all forces related to the torsion potential (Monasse and Boussinot, 2014),

$$\tilde{\mathbf{M}} = \mathbf{x}_i \times \tilde{\mathbf{F}}^{i,jkl}_{\text{dihedral}} + \mathbf{x}_l \times \tilde{\mathbf{F}}^{l,ijk}_{\text{dihedral}} + \mathbf{x}_k \times \tilde{\mathbf{F}}^{k,ijl}_{\text{dihedral}} + \mathbf{x}_j \times \tilde{\mathbf{F}}^{j,ikl}_{\text{dihedral}} = 0. \tag{31}$$

4. Potentials and forces related to non-bonded interactions

4.1. Van der Waals forces and hydrogen bonds

So-called non-electrostatic weak chemical bonds (which are sometimes referred to as intermolecular forces), comprising van der Waals forces and hydrogen bonds, account for interactions between atoms which are not directly linked by any kind of bonding potential. For quantifying the related potential, the Lennard-Jones (LJ) potential has turned out as reasonable approximation, reading as (Ivani, 2016; Swails, 2013)

$$\tilde{E}^{ij}_{\text{LJ}} = \frac{a_{i,j}}{|r_{ij}|^{12}} - \frac{b_{i,j}}{|r_{ij}|^{6}}, \tag{32}$$

where $a_{i,j}$ and $b_{i,j}$ are two parameters which follow from the considered force field. The related force acting on atom i, with position $\mathbf{x}_i$, stemming from the non-electrostatic weak chemical bond interactions between atoms i and j reads as (Monasse and Boussinot, 2014)

$$\tilde{\mathbf{F}}^{i,j}_{\text{LJ}} = \left(\frac{12\, a_{i,j}}{|r_{ij}|^{13}} - \frac{6\, b_{i,j}}{|r_{ij}|^{7}}\right) \mathbf{n}_{ji}. \tag{33}$$

Furthermore, considering a group of four atoms (denoted by indices i, j, k, and l) forming together a dihedral angle, the potential generated through the non-electrostatic weak chemical bond interaction between the first atom i and the last atom l of such a group is also quantified via the LJ potential, however divided by a scaling factor s^{ijkl}_{LJ} (Swails, 2013; Swails et al., 2013),

$$\tilde{E}^{ijkl}_{\text{LJ},1-4} = \frac{\tilde{E}^{il}_{\text{LJ}}}{s^{ijkl}_{\text{LJ}}}, \tag{34}$$

where s_{LJ}^{ijkl} follows from the considered force field. Analogously, the corresponding force follows as

$$\tilde{\mathbf{F}}_{\mathrm{LJ},1-4}^{i,l} = \frac{\tilde{\mathbf{F}}_{\mathrm{LJ}}^{i,l}}{s_{\mathrm{LJ}}^{ijkl}} \,. \tag{35}$$

Notably, $\tilde{E}_{\mathrm{LJ},1-4}^{ijkl}$ and $\tilde{\mathbf{F}}_{\mathrm{LJ},1-4}^{i,l}$ only apply if the interaction between atoms i and l is not already considered by another stretching, bending, or torsion potential.

4.2. Electrostatic interactions

Considering two electrically charged atoms i and j which are not directly linked by any kind of bonding potential with each other, the Coulomb potential describing the electrostatic potential between these two atoms reads as (Ivani, 2016; Swails, 2013; Swails et al., 2013)

$$\tilde{E}_{\mathrm{charge}}^{ij} = \frac{1}{r_{ij}} k_{\mathrm{C}} Q_i Q_j \,, \tag{36}$$

where Q_i and Q_j are the point charges of atoms i and j and k_{C} is the Coulomb constant, $k_{\mathrm{C}} = 332.05$ Å kcal/(mol q_{e}^2), (Case, 2019) with q_{e} being the elementary charge $q_{\mathrm{e}} = 1.602\,176\,634 \times 10^{-19}$ C (von Klitzing, 2019). The corresponding force acting on atom i, with position $\mathbf{x}_i$, stemming from the Coulomb force between atoms i and j, reads as

$$\tilde{\mathbf{F}}_{\mathrm{charge}}^{i,j} = -\frac{\mathrm{d}\tilde{E}_{\mathrm{charge}}^{ij}}{\mathrm{d}\mathbf{x}_i} = \frac{1}{r_{ij}^2} k_{\mathrm{C}} Q_i Q_j \mathbf{n}_{ji} \,, \tag{37}$$

Furthermore, considering a group of four atoms (denoted by indices i, j, k, and l) forming together a dihedral angle, the potential generated through the electrostatic interaction between the first atom i and the last atom l of such a group is also quantified via the Coulomb potential, however divided by a scaling factor s_{ES}^{ijkl} (Swails, 2013; Swails et al., 2013),

$$\tilde{E}_{\mathrm{charge},1-4}^{ijkl} = \frac{\tilde{E}_{\mathrm{charge}}^{il}}{s_{\mathrm{ES}}^{ijkl}} \,, \tag{38}$$

where s_{ES}^{ijkl} follows from the considered force field. Analogously, the corresponding force follows as

$$\tilde{\mathbf{F}}_{\mathrm{charge},1-4}^{i,l} = \frac{\tilde{\mathbf{F}}_{\mathrm{charge}}^{i,l}}{s_{\mathrm{ES}}^{ijkl}} \,. \tag{39}$$

Thereby, the same restriction as formulated at the end of Section 4.1 applies.

4.3. Generalized Born potential

In order to approximate the molecular electrostatics in the atoms-surrounding solvent, the Generalized Born (GB) model (Hawkins et al., 1995; 1996) is applied, using the parameters provided in (Tsui and Case, 2001). We specify the GB model (i) for a neutral concentration of counter-ions in the solution; (ii) for an interior dielectric constant $\epsilon_{\mathrm{int}} = 1$; and (iii) for an exterior (solvent) dielectric constant $\epsilon_{\mathrm{solvent}} = 78.5$. Then, the general definition of the GB potential, E_{GB}, simplifies to (Case, 2019)

$$\tilde{E}_{\mathrm{GB}}^{1\ldots N_{\mathrm{atom}}} = -\frac{155}{157} \sum_{k=1}^{N_{\mathrm{atom}}} \left(\frac{k_{\mathrm{C}} Q_k^2}{2R_k} + \sum_{l=k+1}^{N_{\mathrm{atom}}} \frac{k_{\mathrm{C}} Q_k Q_l}{\sqrt{r_{kl}^2 + R_k R_l \xi_{kl}}} \right) , \tag{40}$$

where R_k and R_l are the so-called effective Born radii of atoms k and l (Case, 2019). For any atom i, the corresponding effective Born radius R_i is defined as

$$R_i = \left[\left(\sum_{j=1}^{N_{\mathrm{atom}}} K_{\mathrm{eff},i}^{j} \right) + \frac{1}{r_{\mathrm{born},i} - r_{\mathrm{offset}}} \right]^{-1} . \tag{41}$$

In Eq. (41), r_{offset} denotes the uniform Born radii offset, $r_{\mathrm{offset}} = 0.09$ Å, reducing the dielectric radii $r_{\mathrm{born},i}$ to the so-called "intrinsic radii" (Case, 2019), $r_{\mathrm{int},i} = r_{\mathrm{born},i} - r_{\mathrm{offset}}$, whereas the variable $K_{\mathrm{eff},i}$, computed as described further below, represents the curvature change of the effective Born radii. Furthermore, Eq. (40) contains variable ξ_{kl}, which represents the following term:

$$\xi_{kl} = \exp\left(-\frac{r_{kl}^2}{4 R_k R_l} \right) . \tag{42}$$

The force acting onto an individual atom i, located at position $\mathbf{x}_i$ and stemming from the GB model, follows, according to Eq. (6), from the derivative of the GB energy, defined in Eq. (40), with respect to $\mathbf{x}_i$:

$$\tilde{\mathbf{F}}_{\mathrm{GB}}^{i,1\ldots N_{\mathrm{atom}}} = -\frac{d\tilde{E}_{\mathrm{GB}}^{1\ldots N_{\mathrm{atom}}}}{\mathrm{d}\mathbf{x}_i} = -\sum_{j=1}^{N_{\mathrm{atom}}}\left(\frac{d\tilde{E}_{\mathrm{GB}}^{1\ldots N_{\mathrm{atom}}}}{\mathrm{d}r_{ij}}\frac{\mathrm{d}r_{ij}}{\mathrm{d}\mathbf{x}_i}\right) = -\sum_{j=1}^{N_{\mathrm{atom}}}\left(\left[\frac{\partial\tilde{E}_{\mathrm{GB}}^{1\ldots N_{\mathrm{atom}}}}{\partial r_{ij}} + \sum_{k=1}^{N_{\mathrm{atom}}}\left\{\frac{\partial\tilde{E}_{\mathrm{GB}}^{1\ldots N_{\mathrm{atom}}}}{\partial R_k}\frac{\partial R_k}{\partial r_{ij}}\right\}\right]\frac{\mathrm{d}r_{ij}}{\mathrm{d}\mathbf{x}_i}\right). \tag{43}$$

Taking into account that

$$\forall k \neq \{i,j\}: \ \frac{\partial R_k}{\partial r_{ij}} = 0\,, \tag{44}$$

and that

$$\frac{\mathrm{d}r_{ij}}{\mathrm{d}\mathbf{x}_i} = \mathbf{n}_{ji}\,, \tag{45}$$

allows for rewriting Eq. (43), yielding

$$\tilde{\mathbf{F}}_{\mathrm{GB}}^{i,j} = -\frac{\mathrm{d}\tilde{E}_{\mathrm{GB}}^{1\ldots N_{\mathrm{atom}}}}{\mathrm{d}r_{ij}}\cdot\mathbf{n}_{ji} = -\left[\frac{\partial\tilde{E}_{\mathrm{GB}}^{ij}}{\partial r_{ij}} + \frac{\partial\tilde{E}_{\mathrm{GB}}^{i,1\ldots N_{\mathrm{atom}}}}{\partial R_i}\frac{\partial R_i}{\partial r_{ij}} + \frac{\partial\tilde{E}_{\mathrm{GB}}^{j,1\ldots N_{\mathrm{atom}}}}{\partial R_j}\frac{\partial R_j}{\partial r_{ij}}\right]\cdot\mathbf{n}_{ji}\,. \tag{46}$$

The derivative $\mathrm{d}\tilde{E}_{\mathrm{GB}}/\mathrm{d}r_{ij}$, occurring in Eq. (46), is derived as follows:

$$\begin{aligned}\frac{d\tilde{E}_{\mathrm{GB}}^{1\ldots N_{\mathrm{atom}}}}{dr_{ij}} = \frac{155}{314}\Bigg\{&\left(\sum_{l=\{i,j\}}\frac{k_{\mathrm{C}}\,Q_l^2}{R_l^2}\frac{\partial R_l}{\partial r_{ij}}\right)\\ &+k_{\mathrm{C}}\,Q_iQ_j\left[r_{ij}^2+R_iR_j\xi_{ij}\right]^{-3/2}\left[2\,r_{ij}+\xi_{ij}\left\{\frac{r_{ij}}{2}+\left(1+\frac{r_{ij}^2}{4R_iR_j}\right)\left(R_j\frac{\partial R_i}{\partial r_{ij}}+R_i\frac{\partial R_j}{\partial r_{ij}}\right)\right\}\right]\\ &+\sum_{l=\{i,j\}}\left[\sum_{m\in M_1/M_2}\frac{k_{\mathrm{C}}\,Q_lQ_mR_m\xi_{lm}}{\left(r_{lm}^2+R_lR_m\xi_{lm}\right)^{3/2}}\frac{\partial R_l}{\partial r_{ij}}\left(1+\frac{r_{lm}^2}{4\,R_l\,R_m}\right)\right]\Bigg\},\end{aligned} \tag{47}$$

with $M_1=\{1,\ldots,N_{\mathrm{atom}}\}$ and $M_2=\{i,j\}$.

For computation of the aforementioned variable $K_{\mathrm{eff},i}$ as well as its derivation with respect to r_{ij}, six case differentiations based on the geometrical configurations of the involved atoms are required, considering for that purpose r_{offset}, the maximum distance for calculating the effective Born radii, $r_{\mathrm{GB}}^{\max}=25$ Å (Case, 2019), and the so-called field screening parameter $f_{\mathrm{s},ij}$:

- Case 1: If $\left(r_{\mathrm{GB}}^{\max}-f_{\mathrm{s},j}\right) < r_{ij} \leq \left(r_{\mathrm{GB}}^{\max}+f_{\mathrm{s},j}\right)$, then

$$K_{\mathrm{eff},i}^{j} = -\frac{1}{8r_{ij}}\left(1+\frac{2r_{ij}}{r_{ij}-f_{\mathrm{s},j}}+\frac{r_{ij}^2-4r_{\mathrm{GB}}^{\max}r_{ij}-f_{\mathrm{s},j}^2}{\left(r_{\mathrm{GB}}^{\max}\right)^2}+2\log\left[\frac{r_{ij}-f_{\mathrm{s},j}}{r_{\mathrm{GB}}^{\max}}\right]\right), \tag{48}$$

  and

$$\frac{\partial K_{\mathrm{eff},i}^{j}}{\partial r_{ij}} = -\frac{K_{\mathrm{eff},i}^{j}}{r_{ij}}-\frac{1}{8r_{ij}}\left(\frac{2}{r_{ij}-f_{\mathrm{s},j}}\left[2-\frac{r_{ij}}{r_{ij}-f_{\mathrm{s},j}}\right]+\frac{2r_{ij}-4r_{\mathrm{GB}}^{\max}}{\left(r_{\mathrm{GB}}^{\max}\right)^2}\right). \tag{49}$$

- Case 2: If $\left(4f_{\mathrm{s},j}\right) < \left(r_{ij} \leq r_{\mathrm{GB}}^{\max}-f_{\mathrm{s},j}\right)$, then

$$K_{\mathrm{eff},i}^{j} = -\frac{\zeta_{ji}f_{\mathrm{s},j}}{r_{ij}^2}\left(\frac{1}{3}+\frac{2\zeta_{ji}}{5}+\frac{3\zeta_{ji}^2}{7}+\frac{4\zeta_{ji}^3}{9}+\frac{5\zeta_{ji}^4}{11}\right), \tag{50}$$

  whereby $\zeta_{ji}=(f_{\mathrm{s},j}/r_{ij})^2$, and

$$\frac{\partial K_{\mathrm{eff},i}^{j}}{\partial r_{ij}} = \frac{4\zeta_{ji}f_{\mathrm{s},j}}{r_{ij}^3}\left(\frac{1}{3}+\frac{3\zeta_{ji}}{5}+\frac{6\zeta_{ji}^2}{7}+\frac{10\zeta_{ji}^3}{9}+\frac{15\zeta_{ji}^4}{11}\right). \tag{51}$$

- Case 3: If $\left(r_{\mathrm{born},i}-r_{\mathrm{offset}}+f_{\mathrm{s},j}\right) < r_{ij} \leq \min\left[\left(r_{\mathrm{GB}}^{\max}-f_{\mathrm{s},j}\right),\,4f_{\mathrm{s},j}\right]$, then

$$K_{\mathrm{eff},i}^{j} = -\frac{1}{2}\left\{\frac{f_{\mathrm{s},j}}{r_{ij}^2-f_{\mathrm{s},j}^2}+\frac{1}{2r_{ij}}\log\left(\frac{r_{\mathrm{dis},ij}}{r_{ij}+f_{\mathrm{s},j}}\right)\right\}, \tag{52}$$

where $r_{\mathrm{dis},ij}$ is referred to as the discontinuity length, defined as follows:

$$r_{\mathrm{dis},ij} = \begin{cases} r_{ij} - f_{\mathrm{s},j} & \text{if } \left(r_{\mathrm{int},i} + f_{\mathrm{s},j}\right) < r_{ij} \leq 4f_{\mathrm{s},j} \\ r_{\mathrm{int},i} & \text{if } |r_{\mathrm{int},i} - f_{\mathrm{s},j}| < r_{ij} \leq \min\left[(r_{\mathrm{int},i} + f_{\mathrm{s},j}),\ 4f_{\mathrm{s},j}\right] \\ f_{\mathrm{s},j} - r_{ij} & \text{if } \left(r_{\mathrm{int},i}\right) < f_{\mathrm{s},j} \text{ and } r_{ij} \leq \min\left[r_{\mathrm{int},i} + f_{\mathrm{s},j},\ 4f_{\mathrm{s},j},\ |r_{\mathrm{int},i} - f_{\mathrm{s},j}|\right] \\ 1 & \text{if } f_{\mathrm{s},j} \leq \left(r_{\mathrm{int},i}\right) \text{ and } r_{ij} \leq \min\left[r_{\mathrm{int},i} + f_{\mathrm{s},j},\ 4f_{\mathrm{s},j},\ |r_{\mathrm{int},i} - f_{\mathrm{s},j}|\right]. \end{cases} \tag{53}$$

Furthermore, the derivative of $K^j_{\mathrm{eff},i}$ according to Eq. (52), with respect to r_{ij} reads as

$$\frac{\partial K^j_{\mathrm{eff},i}}{\partial r_{ij}} = -\frac{1}{2}\left\{ \frac{-2r_{ij}f_{\mathrm{s},j}}{\left(r_{ij}^2 - f_{\mathrm{s},j}^2\right)^2} - \frac{1}{2r_{ij}^2}\log\left(\frac{r_{\mathrm{dis},ij}}{r_{ij} + f_{\mathrm{s},j}}\right) + \frac{r_{ij} + f_{\mathrm{s},j}}{2r_{ij}r_{\mathrm{dis},ij}}\left(-\frac{r_{\mathrm{dis},ij}}{\left(r_{ij} + f_{\mathrm{s},j}\right)^2} + \frac{\partial r_{\mathrm{dis},ij}}{\partial r_{ij}}\frac{1}{r_{ij} + f_{\mathrm{s},j}}\right)\right\}, \tag{54}$$

with the derivatives of $r_{\mathrm{dis},ij}$ with respect to r_{ij} following straightforwardly from Eq. (53), taking the values 1, 0, −1, and 0, in the sequence of the options as presented in Eq. (53).

- Case 4: If $|r_{\mathrm{int},i} - f_{\mathrm{s},j}| < r_{ij} \leq \min\left[(r^{\max}_{\mathrm{GB}} - f_{\mathrm{s},j}),\ 4f_{\mathrm{s},j},\ (r_{\mathrm{int},i} + f_{\mathrm{s},j})\right]$, then

$$K^j_{\mathrm{eff},i} = -\frac{1}{4}\left(\frac{1}{r_{\mathrm{int},i}}\left[2 - \left\{\frac{r_{ij}^2 + r_{\mathrm{int},i}^2 - f_{\mathrm{s},j}^2}{2r_{\mathrm{int},i}r_{ij}}\right\}\right] - \frac{1}{r_{ij} + f_{\mathrm{s},j}} + \frac{1}{r_{ij}}\log\left(\frac{r_{\mathrm{dis},ij}}{r_{ij} + f_{\mathrm{s},j}}\right)\right), \tag{55}$$

and

$$\frac{\partial K^j_{\mathrm{eff},i}}{\partial r_{ij}} = \frac{1}{8r_{ij}^2}\left[\left(\frac{f_{\mathrm{s},j}}{r_{\mathrm{int},i}}\right)^2 + \frac{2f_{\mathrm{s},j}r_{ij}}{\left(f_{\mathrm{s},j} + r_{ij}\right)^2} - \frac{\partial r_{\mathrm{dis},ij}}{\partial r_{ij}}\frac{2r_{ij}}{r_{\mathrm{dis},ij}} + \left(\frac{r_{ij}}{r_{\mathrm{int},i}}\right)^2 + 2\log\left(\frac{r_{\mathrm{dis},ij}}{r_{ij} + f_{\mathrm{s},j}}\right) - 1\right]. \tag{56}$$

- Case 5: If $r_{\mathrm{int},i} < f_{\mathrm{s},j}$ and $r_{ij} \leq \min\left[(r^{\max}_{\mathrm{GB}} - f_{\mathrm{s},j}),\ 4f_{\mathrm{s},j},\ \left|r_{\mathrm{int},i} - |f_{\mathrm{s},j}|\right|\right]$, then

$$K^j_{\mathrm{eff},i} = -\frac{f_{\mathrm{s},j}}{2\left(r_{ij}^2 - f_{\mathrm{s},j}^2\right)} + \frac{1}{r_{\mathrm{int},i}} + \frac{1}{4r_{ij}}\log\left(\frac{r_{\mathrm{dis},ij}}{r_{ij} + f_{\mathrm{s},j}}\right), \tag{57}$$

and

$$\frac{\partial K^j_{\mathrm{eff},i}}{\partial r_{ij}} = \frac{f_{\mathrm{s},j}r_{ij}}{\left(r_{ij}^2 - f_{\mathrm{s},j}^2\right)^2} + \frac{1}{4r_{ij}}\left[\left(\frac{1}{r_{\mathrm{dis},ij}}\frac{\partial r_{\mathrm{dis},ij}}{\partial r_{ij}} - \frac{1}{r_{ij} + f_{\mathrm{s},j}}\right) - \frac{1}{r_{ij}}\log\left(\frac{r_{\mathrm{dis},ij}}{r_{ij} + f_{\mathrm{s},j}}\right)\right], \tag{58}$$

- Case 6: If neither of the above-defined five cases applies, then $K^j_{\mathrm{eff},i} = 0$ and $\partial K^j_{\mathrm{eff},i}/\partial r_{ij} = 0$.

5. Atom-specific resulting forces and total potential energy of atomic compound

The resulting force to which a single atom i is subjected results from summing up the contributions presented in Sections 3 and 4. To that end, the following summation rule needs to be followed:

$$\begin{aligned} \widetilde{\mathbf{F}}_i^{\mathrm{res}} = \sum_{j=1}^{N_{ij}} \Bigg\{ \widetilde{\mathbf{F}}^{i,j}_{\mathrm{bond}} + \sum_{k=1}^{N_{ijk}} \Bigg[\widetilde{\mathbf{F}}^{i,jk}_{\mathrm{angle}} + \sum_{l=1}^{N_{ijkl}} \left(\widetilde{\mathbf{F}}^{i,jkl}_{\mathrm{dihedral}} + \widetilde{\mathbf{F}}^{i,l}_{\mathrm{charge},1-4} + \widetilde{\mathbf{F}}^{i,l}_{\mathrm{LJ},1-4} \right) \Bigg] \\ + \sum_{h=1}^{N_{hij}} \Bigg[\widetilde{\mathbf{F}}^{i,hj}_{angle} + \sum_{g=1}^{N_{hijg}} \widetilde{\mathbf{F}}^{i,hjg}_{dihedral} \Bigg] \Bigg\} + \sum_{m=1}^{N_{\mathrm{atom}}} \left(\widetilde{\mathbf{F}}^{i,m}_{\mathrm{charge}} + \widetilde{\mathbf{F}}^{i,m}_{\mathrm{LJ}} \right) + \sum_{n=1}^{N_{\mathrm{atom}}} \widetilde{\mathbf{F}}^{i,n}_{\mathrm{GB}}. \end{aligned} \tag{59}$$

In Eq. (59), N_{ij} denotes the number of all atoms j which exhibit a covalent bond with atom i; N_{ijk} denotes the number of all atoms k which form, together with specific atoms i and j, an angle between covalently bonded atoms; N_{ijkl} denotes the number of all atoms l which form, together with specific atoms i, j, and k a dihedral angle; and indices g and h are defined analogously to k and l. As for the latter distinction, it should be noted that for atom groups ijk and $ijkl$, atom i is a corner atom, bonded (within this particular group) only to atom j, whereas it is an interior atom in groups hij and $hijg$, bonded to atoms h and j. Furthermore, the last but one summation in Eq. (59) over index m relates to all atoms in the studied force field, excluding however all atom interactions which have already been considered by any of the other interaction forces (relating to stretching, angle, and torsional potentials), whereas the last summation over index n concerns the entirety of the considered atoms.

Importantly, reiterating from Section 2, $\widetilde{\mathbf{F}}_i^{\mathrm{res}}$ according to Eq. (59) needs to be split up into two contributions, $\widetilde{\mathbf{F}}_i^{\mathrm{int}}$ and $\widetilde{\mathbf{F}}_i^{\mathrm{ext}}$. The underlying principle dictates that a specific force contributes to $\widetilde{\mathbf{F}}_i^{\mathrm{int}}$ if all atoms h, i, j, k, l, m, n are located inside the RLE, whereas it contributes to $\widetilde{\mathbf{F}}_i^{\mathrm{ext}}$ if one or several of the atoms h, i, j, k, l, m, n are located outside the RLE. Finally, it is important to stress that all forces defined in Sections 3 and 4 relate to one mole of the studied atoms. Hence, in order to insert the computed atom forces $\widetilde{\mathbf{F}}_i^{\mathrm{int}}$ and $\widetilde{\mathbf{F}}_i^{\mathrm{ext}}$ into the PVP, see Section 2.2, they need to be divided by the Avogadro number $N_{\mathrm{Av}} = 6.02214076 \times 10^{23}\,\mathrm{mol}^{-1}$ (Güttler et al., 2019; Wood and Bettin, 2019), yielding

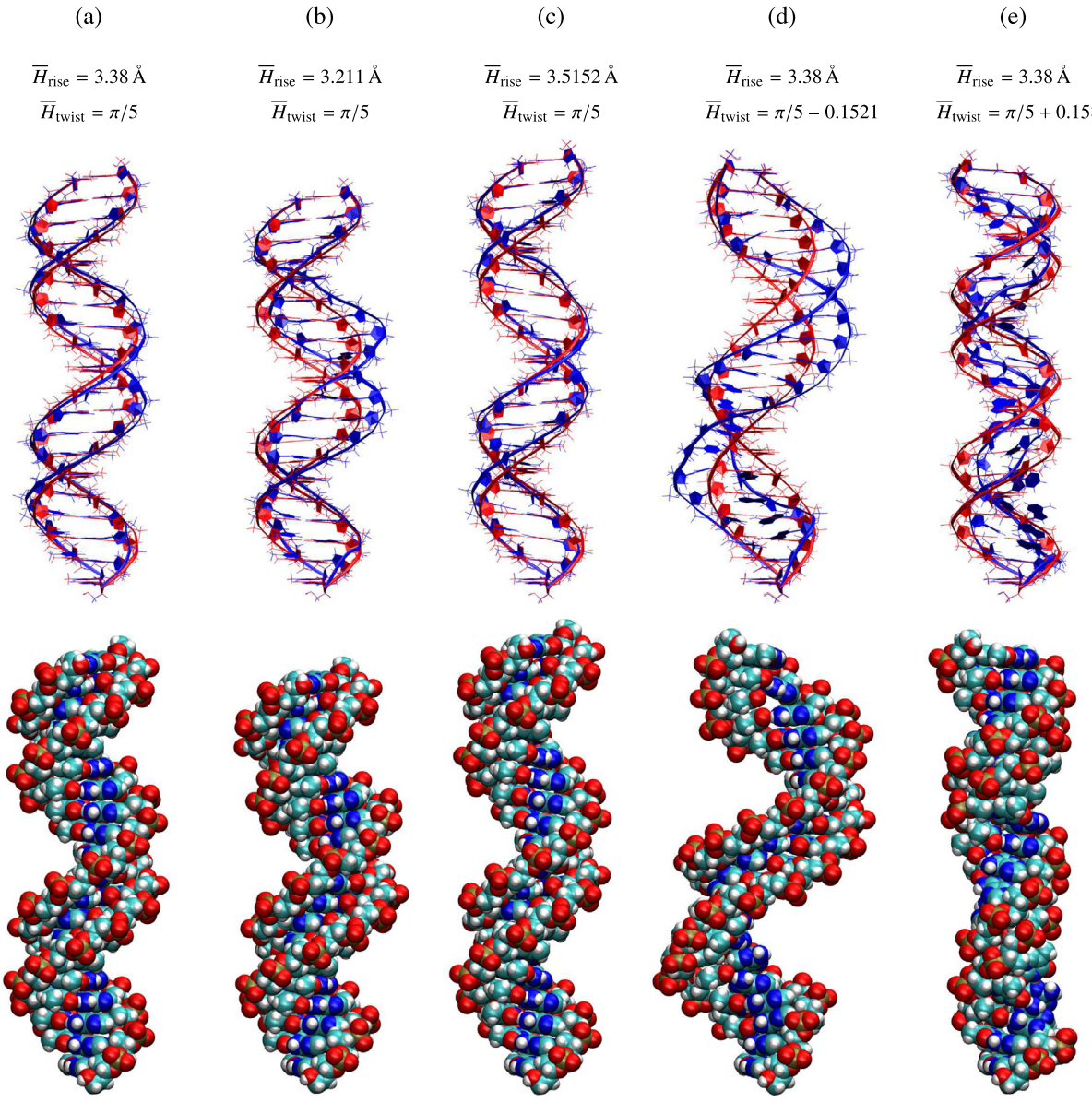

Fig. 3. Molecular dynamics representation of adenine–tyhmine B-DNA, consisting of 20 base pairs. The original configuration is shown in (a), while (b) shows a compressed configuration ($\lambda_x = 0.95$), (c) shows a stretched configuration ($\lambda_x = 1.04$), (d) shows an underwound configuration ($\vartheta_x = -0.45\,\text{rad/nm}$), and (e) shows an overwound configuration ($\vartheta_x = 0.47\,\text{rad/nm}$), including the macroscopic averaged helical rise $\overline{H}_{\text{rise}}$ and helical twist $\overline{H}_{\text{twist}}$. The images in the second line show (in red color) the initial deformed structure according to the homogeneous displacement field dictated by Eq. (63), and (in blue color) the related energy-minimized structures, whereas the images in the first line show the energy-minimized snapshots of the DNA (with cyan indicating carbon atoms, blue indicating nitrogen atoms, red indicating oxygen atoms, white indicating hydrogen atoms, and gold indicating phosphorous atoms). (For interpretation of the references to colour in this figure legend, the reader is referred to the web version of this article.)

$$\mathbf{F}_i^{\text{int}} = \frac{\tilde{\mathbf{F}}_i^{\text{int}}}{N_{\text{Av}}} \quad \text{and} \quad \mathbf{F}_i^{\text{ext}} = \frac{\tilde{\mathbf{F}}_i^{\text{ext}}}{N_{\text{Av}}}\,. \tag{60}$$

The total potential energy of an agglomerate of atoms results from summing up the respective contributions presented in Sections 3 and 4, according to that end, the following summation rule needs to be followed:

$$\tilde{E}_{\text{pot}} = \sum_{ij=1}^{N_{\text{bond}}} \tilde{E}_{\text{bond}}^{ij} + \sum_{ijk=1}^{N_{\text{angle}}} \tilde{E}_{\text{angle}}^{ijk} + \sum_{ijkl=1}^{N_{\text{dihedral}}} \left(\tilde{E}_{\text{dihedral}}^{ijkl} + \tilde{E}_{\text{charge},1-4}^{ijkl} + \tilde{E}_{\text{LJ},1-4}^{ijkl} \right) + \sum_{i=1}^{N_{\text{atom}}} \sum_{m=1}^{N_{\text{atom}}} \left(\tilde{E}_{\text{charge}}^{im} + \tilde{E}_{\text{LJ}}^{im} \right) + \tilde{E}_{\text{GB}}^{1\ldots N_{\text{atom}}}\,. \tag{61}$$

with the number of bonds N_{bond}, the number of angles N_{angle}, the number of dihedrals N_{dihedral} and the energy components $\tilde{E}^{ij}_{\text{bond}}$, $\tilde{E}^{ijk}_{\text{angle}}$, $\tilde{E}^{ijkl}_{\text{dihedral}}$, $\tilde{E}^{ijkl}_{\text{charge},1-4}$, $\tilde{E}^{ijkl}_{\text{LJ},1-4}$, $\tilde{E}^{im}_{\text{charge}}$, $\tilde{E}^{im}_{\text{LJ}}$ and $\tilde{E}^{1\ldots N_{\text{atom}}}_{\text{GB}}$ according to Eqs. (17), (20), (25), (38), (34), (36), (32) and (40).

Conversion of $\tilde{E}_{\text{pot}}$ to the potential energy experienced by one single molecule requires, as introduced above for the atom forces, division of $\tilde{E}_{\text{pot}}$ by N_{Av},

$$E_{\text{pot}} = \frac{\tilde{E}_{\text{pot}}}{N_{\text{Av}}} \,. \tag{62}$$

6. Molecular dynamics model of DNA

For demonstrating the application of the new homogenization approach presented in Sections 2 to 5, poly(dA)-poly(dT)-B-DNA (Herrera and Chaires, 1989; Strauss et al., 1981; Yoo et al., 2001) is studied, also referred to adenine–thymine. The corresponding MD model, comprising 20 base pairs (corresponding to two full turns of the helix in the undeformed configuration) was created using the Nucleic Acid Building (NAB) molecular manipulation language (Macke and Case, 1997), obtaining an initial, helical rise of $H_{\text{rise}} = 3.38$Å and an initial helical twist of $H_{\text{twist}} = \pi/5$ for each base pair, see Fig. 3(a). Thereby, the helical rise of a DNA-strand corresponds to the axial distance of one base to the next one, whereas its helical twist corresponds to the axial rotation of the plane of one base with respect to the neighboring one (Lu and Olson, 2003).

All subsequently described simulations were carried out based on implementing the above-described DNA sequence in Amber18 (Case, 2019), using for that purpose also several of the included tools, such as AmberTools19, including Sander (Case, 2019), and PMEMD (Case, 2019). Moreover, the Parmbsc1 force field (Ivani et al., 2016) was considered. Based on LEaP (Pearlman et al., 1995), which is another tool available in the framework of AmberTools19, the force field-dependent parameters occurring in Sections 3 and 4 were defined. In particular, this concerns the bond term constants k_{ij}, the equilibrium distances r_{eq}, the angle force constants k_{ijk}, the equilibrium angles θ_{eq}, the torsional constants k_{ijkl}, the periodicities $n \in \{1, 2, 3\}$, the phase angles ψ, the LJ parameters pairs $a_{i,j}$ and $b_{i,j}$, the LJ 1–4 scaling factors s^{ijkl}_{LJ}, the point charges Q_i, see (Modeling, 2016); the intrinsic radii $r_{\text{int},i}$, see (Swails et al., 2014); and the field screening parameters $f_{s,j}$, see (Case, 2019).

The studied DNA sequence was subjected, by means of the commercial software Matlab (The MathWorks, 2019), to an initial displacement field $\mathbf{u}(\mathbf{x}_i)$, defining the initial positions of all atoms i before performing the MD simulations. This displacement field allows for introducing constant stretches, and constant twist deformation rates along the longitudinal axis of the helix. Notably, twist deformation rates are defined as the twist rotation per length (Sengupta et al., 2008). Mathematically, $\mathbf{u}(\mathbf{x}_i)$ is defined as follows:

$$\mathbf{u}(\mathbf{x}_i) = \underbrace{(\lambda_x - 1)}_{E_x} x_i^0 \, \mathbf{e}_x + \left[\cos\left(\alpha^0 + \vartheta_x x_i^0\right) \sqrt{(y_i^0)^2 + (z_i^0)^2} - y_i^0 \right] \mathbf{e}_y + \left[\sin\left(\alpha^0 + \vartheta_x x_i^0\right) \sqrt{(y_i^0)^2 + (z_i^0)^2} - z_i^0 \right] \mathbf{e}_z \,, \tag{63}$$

where $\alpha^0 = \arctan(z_i^0/y_i^0)$ is the undeformed angle, $\lambda_x = 1 + (\partial u/\partial X)$ is the axial stretch ratio, $E_x = \lambda_x - 1$ is the stretch, ϑ_x the twist deformation rate in axial direction, and the "undeformed" configuration $\mathbf{x}_i^0 = x_i^0 \, \mathbf{e}_x + y_i^0 \, \mathbf{e}_y + z_i^0 \, \mathbf{e}_z$ as initialized by means of NAB. Several DNA configurations deviating from the originally initialized one were studied; on the one hand axial compression and stretching, implemented via the stretch ratio λ_x, ranging from 0.95, see Fig. 3(b), to 1.04, see Fig. 3(c), while no change of the helical twist was imposed onto the system; and on the other hand axial under- and overwinding, implemented via the axial twist deformation rate ϑ_x, ranging from -0.45 rad/nm, see Fig. 3(d), to 0.47 rad/nm, see Fig. 3(e), while no change of the helical rise was imposed onto the system. The corresponding average helical rises $\overline{H}_{\text{rise}}$ and average helical twists $\overline{H}_{\text{twist}}$ are also indicated in Fig. 3. Furthermore, in all simulations, the first and the last base pair were considered to be spatially restrained. No periodic boundary conditions have been applied the present simulations, hence we used an implicit model (see Section 4.3), without explicit consideration of surrounding atoms.

In order to find conformations which are independent of the initial conformation, the system was first heated up to a temperature of 300 K, using for that purpose a Langevin thermostat (Uberuaga et al., 2004), with different collision frequencies ($0.2\,\text{ps}^{-1}$, $0.5\,\text{ps}^{-1}$ and $1\,\text{ps}^{-1} = 10^{-12}$ s), whereas the time increment in all MD simulations was set to $1\,\text{fs} = 10^{-15}$ s. After being heated up, the system was cooled down to < 1 mK – note that reaching a temperature of exactly 0 K is (computationally) not possible (Palma et al., 2017) – applying then local energy minimization (using for that purpose the steepest gradient method and conjungate gradient search in sequential fashion). This energy minimization procedure was performed with the aforementioned collision frequencies, and different temperatures targeted at heating (300 K, 200 K, 200 K, and 5 times 100 K). The last cooling procedure was split up in three steps, namely (i) cooling from 100 K to 0 K over a time period of 10 000 fs using a collision frequency of $1\,\text{ps}^{-1}$; (ii) an energy minimization using 5000 steepest gradient iterations, and (iii) a 30 000 fs-long MD simulation at < 1 mK using a collision frequency of $0.2\,\text{ps}^{-1}$. Thus, each displacement-controlled load case required a set of MD simulations consisting overall of 170 000 time steps, each of which was 1 fs long. This way, global energy minimization could be achieved in approximated fashion for each of the load cases.

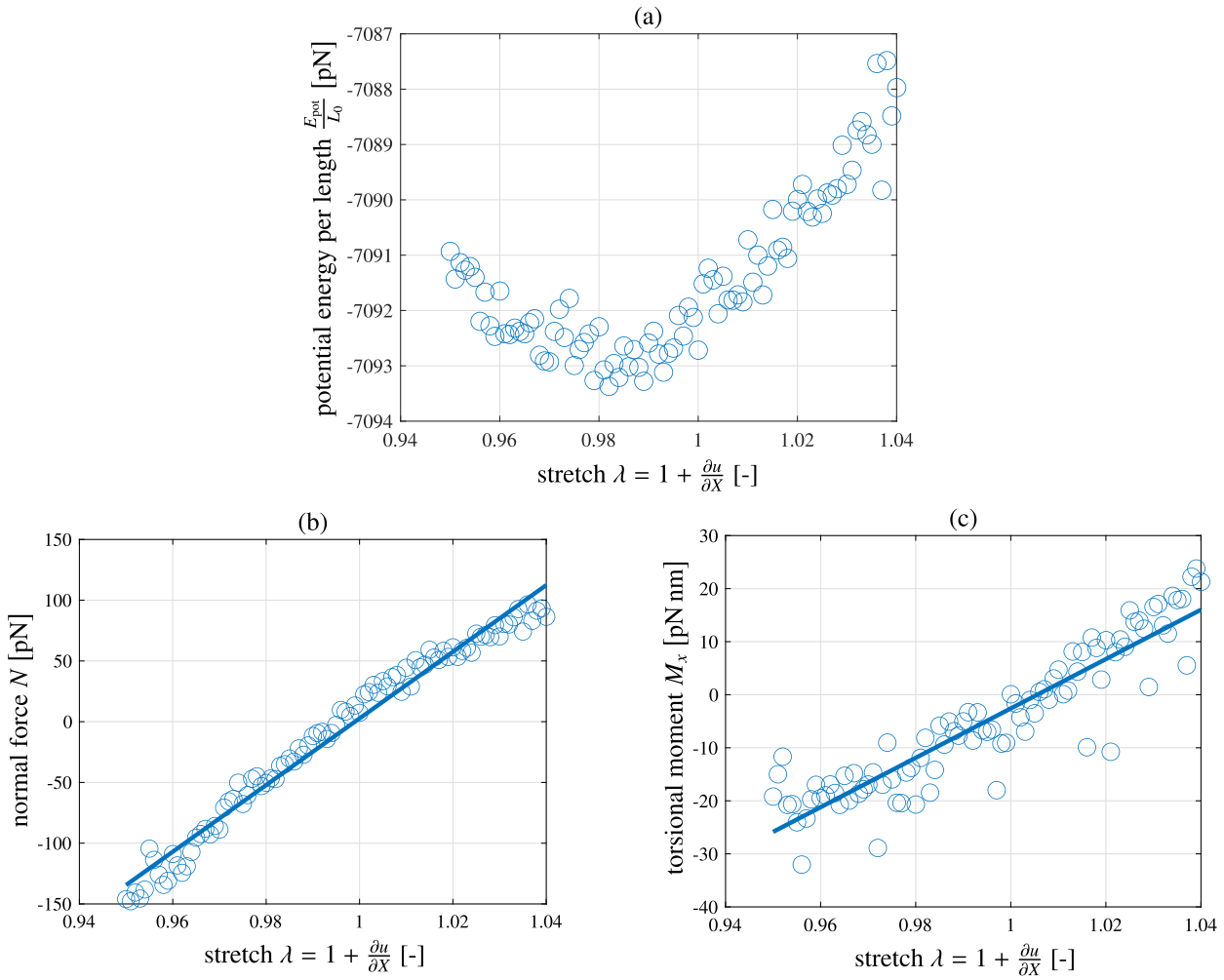

Fig. 4. Results of stretching simulations, illustrated in terms of (a) the potential energy E_{pot} according to Eq. (62), normalized by length L_0 =67.6 Å, over the stretch λ, (b) the normal force N over λ, and (c) the torsional moment M_x over λ.

7. Numerical results

7.1. Simulation of stretching and twisting regimes

First, we present the results of the *in silico* stretching and twisting experiments defined in Section 6, see also Fig. 3 for some examples of the thereby obtained DNA configurations. Fig. 4 shows the results obtained for the stretching simulations, while Fig. 5 shows the results obtained for the twisting simulations.

Fig. 4 (a) shows the potential energy E_{pot} normalized by L_0, which is the length of the originally initialized DNA sequence before altering the configuration by means of Eq. (63), versus the axial stretch λ. Furthermore Figs. 4(b) and (c) show the force quantities N and M_x over λ, making use of the homogenization relations defined in Section 2.3. Furthermore, Figs. 4(b) and (c) also include the linear regressions (based on standard least squares fitting procedures) of the N-over-λ and the M_x-over-λ relations. These straight lines are, in an approximate sense, indicative of the structural stiffnesses of the studied DNA sequences. This way, we can deduce from Fig. 4(b) that the stretching stiffness for a uniaxial stretch amounts to $K = \mathrm{d}N/\mathrm{d}\lambda = 2743\,\text{pN}$, whereas Fig. 4(c) suggests that the stretching-related warping stiffness amounts to $W_{E_x} = \mathrm{d}M_x/\mathrm{d}\lambda = 465\,\text{pN nm}$.

Analogously, Fig. 5(a) shows E_{pot}/L_0 versus the axial twist ϑ_x, while Fig. 5(b) and (c) show N and M_x versus ϑ_x. Interestingly, Fig. 5(a) clearly show three distinctive regimes, which we have termed standard B-DNA conformation (for $-0.21\,\text{rad/nm} \leq \vartheta_x \leq 0.16\,\text{rad/nm}$), underwound conformation (for $-0.45\,\text{rad/nm} \leq \vartheta_x \leq -0.22\,\text{rad/nm}$), and overwound conformation (for $0.12\,\text{rad/nm} \leq \vartheta_x \leq 0.47\,\text{rad/nm}$). Each of these conformations has been subjected to linear fitting, indicating again respective structural stiffnesses. Namely, Fig. 5(b) reveals twisting-related warping stiffnesses of $W_{\vartheta_x} = \mathrm{d}N/\mathrm{d}\vartheta_x = -80\,\text{pN nm}$ for the underwound conformation, of $W_{\vartheta_x} = 373\,\text{pN nm}$ for the standard conformation, and of $W_{\vartheta_x} = -213\,\text{pN nm}$ for the overwound conformation. Remarkably, this means that for both underwound and overwound conformations, we ob-

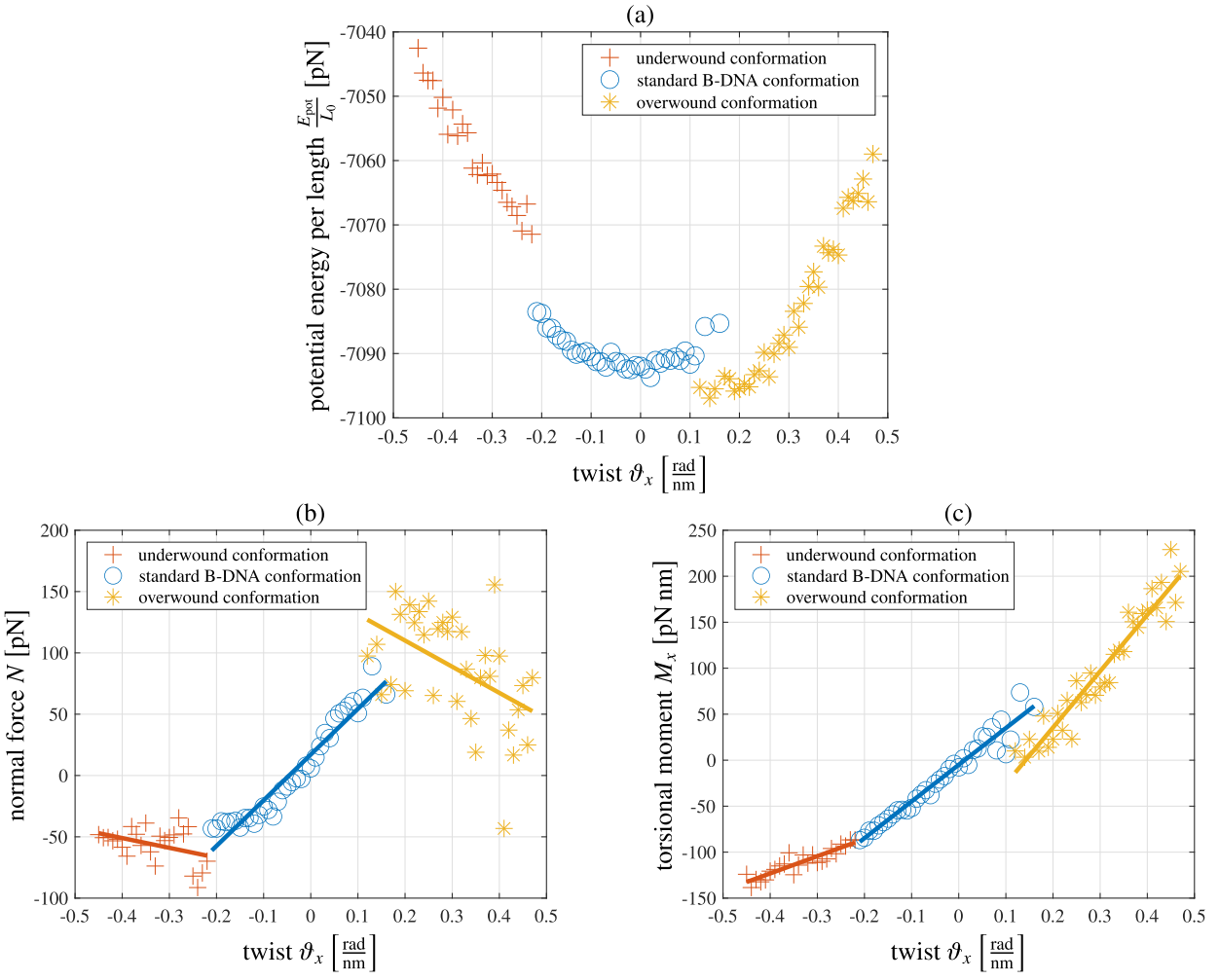

Fig. 5. Results of twisting simulations, illustrated in terms of (a) the potential energy E_{pot} according to Eq. (62), normalized by length L_0=67.6 Å, over the twist ϑ_x, (b) the normal force N over ϑ_x, and (c) the torsional moment M_x over ϑ_x.

serve stretching due to overwinding, as revealed by experiments (Gore et al., 2006). On the other hand, Fig. 5(c) gives access to torsional stiffnesses of $T = \mathrm{d}M_x/\mathrm{d}\vartheta_x = 187\,\mathrm{pN\,nm^2}$ for the underwound conformation, of $T = 399\,\mathrm{pN\,nm^2}$ for the standard configuration, and of $T = 612\,\mathrm{pN\,nm^2}$ for the overwound conformation.

It should be noted that for a more profound, theoretically well-substantiated back-analysis of structural stiffnesses, a rigorous introduction of small- or large-strain kinematics is indispensable. However, this goes beyond the scope of the present paper.

7.2. Comparison with experiments

The simulations presented in this paper were either based on a uniform stretch boundary condition (while $\vartheta_x = 0$) or a uniform twist boundary condition (while $\lambda = 0$). However, experiments accessible in literature usually use boundary conditions involving constant normal forces or constant torsional moments. Hence, in order to compare the results presented in Section 7.1 to those experimental results, a reinterpretation of the computed structural stiffnesses is necessary. To that end, we make use of the following relation, which we deem valid only if the DNA exhibits its standard conformation:

$$\begin{pmatrix} \mathrm{d}N \\ \mathrm{d}M_x \end{pmatrix} = \begin{bmatrix} \frac{\mathrm{d}N}{\mathrm{d}\lambda} & \frac{\mathrm{d}N}{\mathrm{d}\vartheta_x} \\ \frac{\mathrm{d}M_x}{\mathrm{d}\lambda} & \frac{\mathrm{d}M_x}{\mathrm{d}\vartheta_x} \end{bmatrix} \begin{pmatrix} \mathrm{d}E_x \\ \mathrm{d}\vartheta_x \end{pmatrix} = \begin{bmatrix} K & W_{\vartheta_x} \\ W_{E_x} & T \end{bmatrix} \begin{pmatrix} \mathrm{d}E_x \\ \mathrm{d}\vartheta_x \end{pmatrix}. \tag{64}$$

Inverting the expression given in Eq. (64) yields

$$\begin{pmatrix} \mathrm{d}E_x \\ \mathrm{d}\vartheta_x \end{pmatrix} = \frac{1}{KT - W_{\vartheta_x} W_{E_x}} \begin{bmatrix} T & -W_{\vartheta_x} \\ -W_{E_x} & K \end{bmatrix} \begin{pmatrix} \mathrm{d}N \\ \mathrm{d}M_x \end{pmatrix}. \tag{65}$$

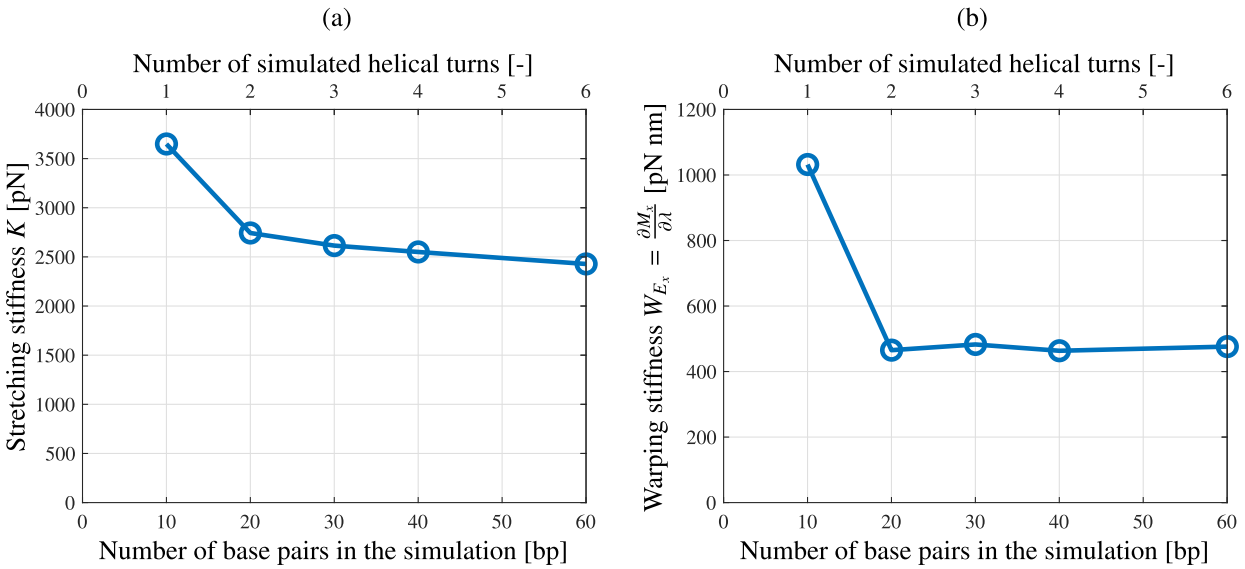

Fig. 6. Dependence of (a) the stretching stiffness K and (b) the stretching-related warping stiffness W_{E_x} on the length of the simulated DNA sequence.

Specifying the first row of Eq. (65) for $\mathrm{d}M_x = 0$ (which relates to an experiment where the DNA is subjected to a normal force, while the torsional moment is equal to zero) leads to

$$\mathrm{d}N = \left(K - \frac{W_{E_x} W_{\vartheta_x}}{T} \right) \mathrm{d}E_x \,, \tag{66}$$

whereby the term in brackets can be interpreted as the related stretching stiffness S. Evaluating this relation for the structural stiffness derived in Section 7.1 yields $S = 2308$ pN. This value slightly exceeds the corresponding values typically suggested in literature, ranging from 476 pN to 2120 pN (Baumann et al., 1997; Ouldridge et al., 2011; Podgornik et al., 2000; Wang et al., 1997; Wu et al., 2015). This discrepancy may be due to the fact that the experimentally studied DNA sequences were 30 to 100 times longer than the ones studied computationally in this paper. It is well known that shorter structures tend to appear stiffer than longer structures made of the same material.

Specifying the second row of Eq. (65) for $\mathrm{d}N = 0$ yields

$$\mathrm{d}M_x = \left(T - \frac{W_{E_x} W_{\vartheta_x}}{K} \right) \mathrm{d}\vartheta_x \,, \tag{67}$$

whereby the term in brackets can be interpreted as the related torsional stiffness C. Evaluating this relation again for the structural stiffnesses derived in Section 7.1 yields $C = 336\,\mathrm{pN\,nm^2}$. This value agrees well with the torsional stiffnesses of DNA provided by literature, ranging from $61\,\mathrm{pN\,nm^2}$ to $480\,\mathrm{pN\,nm^2}$ (Bryant et al., 2003; Crothers et al., 1992; Kim and Kim, 2016; Moroz and Nelson, 1997; Peters et al., 2013).

7.3. Structural size effect

Finally, we study the effect of the DNA length on the resulting structural stiffnesses, considering for that purpose DNA lengths ranging from 10 base pairs (relating to one full helical turn) to 60 base pairs (relating to six full helical turns), see Fig. 6. Both the ratio $\mathrm{d}N/\mathrm{d}\lambda$ (which is again interpreted as stretching stiffness) and the ratio $\mathrm{d}M_x/\mathrm{d}\lambda$ (which is again interpreted as stretching-related warping stiffness) decrease with increasing DNA length, and it seems that both ratios have somewhat converged at a length of 20 base pairs, corroborating the significance of the simulations presented in Section 7.1. This effect is well known as structural size effect (Bažant, 2000; Bažant and Sun, 1987).

In this context, we choose to mention the well-known separation of scales-requirement, on the basis of which the concept of continuum micromechanics has been established (Hill, 1963; 1965; Zaoui, 2002). This requirement clarifies the distinction between the characteristic length of a representative volume element (RVE), ℓ, and the characteristic lengths of the microheterogeneities within this RVE, d; namely, $d \ll \ell$. It has been shown (Drugan and Willis, 1996) that this requirement is already sufficiently well fulfilled if the factor between d and ℓ amounts to approximately 2. Considering that the characteristic length of the microheterogeneity within the DNA structure relates to one full turn of the helix, the above-discussed outcome, namely that convergence of the structural size effect is already reached at a length of two full turns of the helix, confirms that the principle of scale separation is also valid for DNA-type structures.

8. Conclusions and perspectives

The atom-to-beam homogenization approach proposed in this paper is the first documented attempt of directly interpreting results from molecular dynamics simulations within a principle of virtual power-based theoretical framework. In this sense, we further extend the large application range of the PVP, beyond structural mechanics derived from 3D continuum mechanics (Höller et al., 2019; Touratier, 1991), homogenization of eigenstressed microheterogeneous materials (Königsberger et al., 2020), or virtual fields used for elastic parameter identification (Grüdiac et al., 2006). This way, we were able to compute well-established structural stiffness properties of the studied DNA structures, such as stretching, torsional, and warping stiffnesses. We regard this as a valuable conceptual extension of the state of the art in the field of bio-macromolecular MD, defined by landmark papers such as (Buehler, 2006; Keten et al., 2010).

Remarkably, once the coupled force-deformation characteristics at the beam level are quantified, they can be upscaled further, not only to naturally occurring configurations, but also to man-made origami structures (Bai et al., 2012; Castro et al., 2011; Rothemund, 2006). In the long run, this research holds the promise to effectively target (epi-) genetic pathologies stemming from conformational restrictions of the DNA (Champoux, 2001; Garcia-Diaz and Kunkel, 2006; Poli et al., 2005; Portella et al., 2013). This is fully consistent with the ongoing scientific discussion on the "mechanobiome" (Kothari et al., 2019); in more detail, the present results constitute the first step towards defining key nuclear structural elements of this very mechanobiome.

Declaration of Competing Interest

The authors declare that they have no conflict of interest.

Acknowledgments

The authors acknowledge GPU time with the Vienna Scientific Cluster (VSC); and the first author thanks Robert Plachy for fruitful discussions providing helpful insights.

Appendix A List of symbols

$a_{i,j}$	$\mathrm{L}^{14}\,\mathrm{M}\,\mathrm{T}^{-2}\,\mathrm{N}^{-1}$	Parameter of the Lennard-Jones potential according to the force field, introduced in Eq. (32)
$b_{i,j}$	$\mathrm{L}^{8}\,\mathrm{M}\,\mathrm{T}^{-2}\,\mathrm{N}^{-1}$	Parameter of the Lennard-Jones potential according to the force field, introduced in Eq. (32)
C	$\mathrm{L}^{3}\,\mathrm{M}\,\mathrm{T}^{-2}$	Torsional stiffness for $N = 0$-restrainment, defined in Eq. (67)
$\mathbf{e}_x, \mathbf{e}_y, \mathbf{e}_z$	-	Base vectors of a Cartesian coordinate system, were $\mathbf{e}_x$ points into the longitudinal direction and $\mathbf{e}_y$ and $\mathbf{e}_z$ span the cross section, introduced in Eq. (9)
$\tilde{E}^{ijk}_{\mathrm{angle}}$	$\mathrm{L}^{2}\,\mathrm{M}\,\mathrm{T}^{-2}\,\mathrm{N}^{-1}$	Angle potential, defined in Eq. (20)
$\tilde{E}^{ij}_{\mathrm{bond}}$	$\mathrm{L}^{2}\,\mathrm{M}\,\mathrm{T}^{-2}\,\mathrm{N}^{-1}$	Bond potential, defined in Eq. (17)
$\tilde{E}^{ij}_{\mathrm{charge}}$	$\mathrm{L}^{2}\,\mathrm{M}\,\mathrm{T}^{-2}\,\mathrm{N}^{-1}$	Electrostatic potential, defined in Eq. (36)
$\tilde{E}^{ij}_{\mathrm{LJ}}$	$\mathrm{L}^{2}\,\mathrm{M}\,\mathrm{T}^{-2}\,\mathrm{N}^{-1}$	Lennard-Jones potential, defined in Eq. (32)
E_{pot}	$\mathrm{L}^{2}\,\mathrm{M}\,\mathrm{T}^{-2}$	Potential energy, defined in Eq. (62)
$\tilde{E}_{\mathrm{pot}}$	$\mathrm{L}^{2}\,\mathrm{M}\,\mathrm{T}^{-2}\,\mathrm{N}^{-1}$	Potential energy, defined in Eq. (61)
$\tilde{E}_{\mathrm{dihedral}}$	$\mathrm{L}^{2}\,\mathrm{M}\,\mathrm{T}^{-2}\,\mathrm{N}^{-1}$	Dihedral energy, defined in Eq. (25)
$\tilde{E}^{ij}_{\mathrm{GB}}$	$\mathrm{L}^{2}\,\mathrm{M}\,\mathrm{T}^{-2}\,\mathrm{N}^{-1}$	Electrostatic generalized Born energy coefficient relating mainly to atom i and atom j, defined in Eq. (40)
$\tilde{E}^{1\ldots N_{\mathrm{atom}}}_{\mathrm{GB}}$	$\mathrm{L}^{2}\,\mathrm{M}\,\mathrm{T}^{-2}\,\mathrm{N}^{-1}$	Electrostatic generalized Born energy, defined in Eq. (40)
$\tilde{E}^{ijkl}_{\mathrm{charge},1-4}$	$\mathrm{L}^{2}\,\mathrm{M}\,\mathrm{T}^{-2}\,\mathrm{N}^{-1}$	1-4 electrostatic potential, defined in Eq. (38)
$\tilde{E}^{ijkl}_{\mathrm{LJ},1-4}$	$\mathrm{L}^{2}\,\mathrm{M}\,\mathrm{T}^{-2}\,\mathrm{N}^{-1}$	1-4 Lennard-Jones potential, defined in Eq. (34)
E_x	-	Stretch in axial direction; defined in Eq. (63)
$f_{s,i}$	L	Field screening parameter of atom i, according to the force field, introduced in Eqs. (48)–(58)
$\mathbf{F}^{\mathrm{int}}_i$	$\mathrm{L}\,\mathrm{M}\,\mathrm{T}^{-2}$	Internal forces per atom, defined in Eq. (60)
$\tilde{\mathbf{F}}^{\mathrm{int}}_i$	$\mathrm{L}\,\mathrm{M}\,\mathrm{T}^{-2}\,\mathrm{N}^{-1}$	Internal forces per mol of $\tilde{\mathbf{F}}^{\mathrm{res}}_i$ if all atoms h, i, j, k, l, m, n are located inside the RLE.
$\tilde{\mathbf{F}}^{i,1\ldots N_{\mathrm{atom}}}_{\mathrm{GB}}$	$\mathrm{L}\,\mathrm{M}\,\mathrm{T}^{-2}\,\mathrm{N}^{-1}$	Generalized Born force acting on atom i, defined in Eq. (43)
$\tilde{\mathbf{F}}^{i,j}_{\mathrm{GB}}$	$\mathrm{L}\,\mathrm{M}\,\mathrm{T}^{-2}\,\mathrm{N}^{-1}$	Generalized Born force acting between atom i and atom j, involving to all atoms, defined in Eq. (46)
$\tilde{\mathbf{F}}^{i,j}_{\mathrm{bond}}$	$\mathrm{L}\,\mathrm{M}\,\mathrm{T}^{-2}\,\mathrm{N}^{-1}$	Force acting on atom i, due to a stretch potential between atoms i and j, defined in Eq. (19)
$\tilde{\mathbf{F}}^{i,j}_{\mathrm{charge}}$	$\mathrm{L}\,\mathrm{M}\,\mathrm{T}^{-2}\,\mathrm{N}^{-1}$	Coulomb force action on atom i, due to interaction with atom j, defined in Eq. (37)
$\tilde{\mathbf{F}}^{i,l}_{\mathrm{charge},1-4}$	$\mathrm{L}\,\mathrm{M}\,\mathrm{T}^{-2}\,\mathrm{N}^{-1}$	Reduced Coulomb-force acting on atom i, due to atom l, defined in Eq. (39)
$\tilde{\mathbf{F}}^{i,j}_{\mathrm{LJ}}$	$\mathrm{L}\,\mathrm{M}\,\mathrm{T}^{-2}\,\mathrm{N}^{-1}$	Lennard-Jones force acting on atom i, from interaction with atom j, defined in Eq. (33)
$\tilde{\mathbf{F}}^{i,l}_{\mathrm{LJ},1-4}$	$\mathrm{L}\,\mathrm{M}\,\mathrm{T}^{-2}\,\mathrm{N}^{-1}$	Reduced Lennard-Jones force acting on atom i, from interaction with atom l, defined in Eq. (35)
$\tilde{\mathbf{F}}^{i,jk}_{\mathrm{angle}}$	$\mathrm{L}\,\mathrm{M}\,\mathrm{T}^{-2}\,\mathrm{N}^{-1}$	Force acting on atom i, due to an angle potential of atoms i, j and k, defined in Eqs. (21)–(23)
$\tilde{\mathbf{F}}^{i,jkl}_{\mathrm{dihedral}}$	$\mathrm{L}\,\mathrm{M}\,\mathrm{T}^{-2}\,\mathrm{N}^{-1}$	Force in atom i due to an dihedral potential of atoms i, j, k and l, defined in Eqs. (27)–(30)
$\mathbf{F}^{\mathrm{ext}}_i$	$\mathrm{L}\,\mathrm{M}\,\mathrm{T}^{-2}$	External forces per atom, defined in Eq. (60)
$\tilde{\mathbf{F}}^{\mathrm{ext}}_i$	$\mathrm{L}\,\mathrm{M}\,\mathrm{T}^{-2}\,\mathrm{N}^{-1}$	External forces of $\tilde{\mathbf{F}}^{\mathrm{res}}_i$ if one or several of the atoms h, i, j, k, l, m, n

(*continued on next page*)

$\tilde{\mathbf{F}}_i^{\text{res}}$	$\mathrm{L\,M\,T^{-2}\,N^{-1}}$	Resulting force of a single atom i, defined in Eq. (59)
K	$\mathrm{L\,M\,T^{-2}}$	Stretching stiffness of dsDNA for $\vartheta = 0$-restrainment, defined in Eq. (64)
k_c	$\mathrm{L^3\,M\,T^3\,N^{-1}\,I^{-1}}$	Coulomb constant
$K_{\text{eff},i}$	$\mathrm{L^{-1}}$	Reciprocal Born radius change, defined in Eqs. (48)–(57)
k_{ij}	$\mathrm{M\,T^{-2}\,N^{-1}}$	Bond force constant, introduced in Eq. (17)
k_{ijk}	$\mathrm{M\,T^{-2}\,N^{-1}}$	Bending force constant, introduced in Eq. (20)
k_{ijkl}	$\mathrm{M\,T^{-2}\,N^{-1}}$	Dihedral force constant, introduced in Eq. (25)
L	L	Length of the DNA, introduced in Eq. (1)
ℓ_{RLE}	L	Length of representative line element, introduced in Eq. (7)
n	-	Periodicity of the dihedral potential, according to the force field.
$\mathbf{n}_{ij}$	L	Unit vector from atom i to atom j, defined in Eq. (19)
n_x	$\mathrm{M\,T^{-2}}$	Axial line load, introduced in Eq. (2)
N	$\mathrm{L\,M\,T^{-2}}$	Normal force, defined in Eq. (13)
N_{Av}	$\mathrm{N^{-1}}$	Avogadro constant.
N_{atom}	-	Number of atoms in the RLE, introduced in Eq. (7)
m_x	$\mathrm{M\,T^{-2}}$	Torsional moment per length, introduced in Eq. (2)
M_x	$\mathrm{L^2\,M\,T^{-2}}$	Torsional moment, defined in Eq. (14)
$p_{\text{int}}^{\text{atom}}$	$\mathrm{L\,M\,T^{-3}}$	Integrand of the virtual power of internal forces for atomic system, defined in Eq. (7)
$p_{\text{int}}^{\text{cont}}$	$\mathrm{L\,M\,T^{-3}}$	Integrand of the virtual power of internal forces for continuum beam, defined in Eq. (4)
$p_{\text{ext}}^{\text{atom}}$	$\mathrm{L\,M\,T^{-3}}$	Integrand of the virtual power of external forces for atomic system, defined in Eq. (8)
$p_{\text{ext}}^{\text{cont}}$	$\mathrm{L\,M\,T^{-3}}$	Integrand of the virtual power of external forces for continuum beam, defined in Eq. (5)
$\mathcal{P}_{\text{int}}^{\text{cont}}$	$\mathrm{L^2\,M\,T^{-3}}$	Virtual power of internal forces, defined in Eq. (1)
$\mathcal{P}_{\text{ext}}^{\text{cont}}$	$\mathrm{L^2\,M\,T^{-3}}$	Virtual power of external forces, defined in Eq. (2)
q_i	$\mathrm{L^{\frac{3}{2}}\,M^{\frac{1}{2}}\,T^{-1}\,N^{-\frac{1}{2}}}$	Partial charge Q_i multiplied by the square root of the Coulomb constant, defined in Eq. (36)
Q_i	T I	Partial charge, used in Eq. (36)
$r_{\text{dis},ij}$	L	Discontinuity length, see Eqs. (53)
r_{eq}	L	Equilibrium distance according to the force field, defined in Eq. (17)
r_{ij}	L	Distance between atom i and j, defined in Eq. (18)
$r_{\text{int},i}$	L	Intrinsic radius of atom i
$\mathbf{r}_{ij}$	L	Vector from atom i to j, defined in Eq. (18)
$r_{\text{born},i}$	L	Intrinsic radii of atom i
$r_{\text{GB}}^{\text{max}}$	L	Maximum distance for calculating the effective Born radii.
r_{offset}	L	Uniform Born radii offset
R_i	L	Depended effective Born radii of atom i, defined in Eq. (41)
S	$\mathrm{L\,M\,T^{-2}}$	Stretching stiffness of dsDNA for $M_x = 0$-restrainment, defined in Eq. (66)
s_{ES}^{ijkl}	-	Scaling factor for the electrostatic potential, according to the force field, introduced in Eq. (38)
s_{LJ}^{ijkl}	-	Scaling factor for the LJ Potential, according to the force field, introduced in Eq. (34)
T	$\mathrm{L^3\,M\,T^{-2}}$	Torsional stiffness for $E_x = 0$-restrainment, defined in Eq. (64)
$\mathbf{u}$	$\mathrm{L\,M\,T^{-2}}$	Initial displacement field, defined in Eq. (63)
$\hat{\mathbf{v}}^{\text{int}}$	$\mathrm{L\,T^{-1}}$	Virtual velocity vector of atom i for the internal forces, defined in Eq. (9)
$\hat{\mathbf{v}}^{\text{ext}}$	$\mathrm{L\,T^{-1}}$	Virtual velocity vector of atom i for the external forces, defined in Eq. (10)
$\hat{V}$	$\mathrm{L\,T^{-1}}$	Axial virtual velocity in the center of the cross section, introduced in Eq. (1)
W	$\mathrm{L^2\,M\,T^{-2}}$	Warping stiffness, defined in Eqs. (64)
x_i, y_i, z_i	L	Cartesian components of the location vector of atom i, introduced in Eq. (9)
$\mathbf{x}_i$	L	Location vector of atom i $\mathbf{x}_i = x_i \cdot \mathbf{e}_x + y_i \cdot \mathbf{e}_y + z_i \cdot \mathbf{e}_z$, introduced in Eq. (7)
X, Y, Z	L	Cartesian components of the location vector of a beam-point, introduced in Eq. (1)
$\mathbf{X}$	L	Location vector of a beam-point, $\mathbf{X} = X \cdot \mathbf{e}_x + Y \cdot \mathbf{e}_y + Z \cdot \mathbf{e}_z$, introduced in Eq. (1)
Δr	L	Relative distance to the equilibrium distance, defined in Eq. (17)
$\Delta\theta$	-	Relative angle to the equilibrium angle, defined in Eq. (20)
ϵ_{int}	-	Interior dielectric constant
$\epsilon_{\text{solvent}}$	-	Solvent dielectric constant
ζ_{ji}	-	Square ratio between the field screening parameter $f_{s,j}$ and the distance r_{ij}
η	-	Variable, determinating if dihedral is linear
θ_{eq}	-	Equilibrium angle between two bonds, according to the force field, introduced in Eq. (20)
θ_{ijk}	-	Angle between two bounds, defined in Eq. (20)
ϑ_x	$\mathrm{L^{-1}}$	Twist in axial direction, defined in Eq. (63)
λ	-	Stretch ratio, defined in Eq. (63)
ξ_{kl}	-	Exponential variable, defined in Eq. (42)
ψ		Equilibrium torsional angle
ϕ	-	Current torsional angle
$\hat{\Omega}$	$\mathrm{T^{-1}}$	Virtual axial rotational velocity vector, introduced in Eq. (9)

References

Allen, M.P., 2004. Introduction to Molecular Dynamics simulation. In: Attig, N., Binder, K., Grubmüller, H., Kremer, K.D. (Eds.), Computational Soft Matter: From Synthetic Polymers to Proteins. In: NIC series, 23. NIC-Directors, Jülich, pp. 1–28. [Online; accessed 11. April 2019]. https://dasher.wustl.edu/chem478/reading/md-intro-2.pdf

Allen, M.P., Tildesley, D.J., 2017. Computer Simulation of Liquids, Second ed. Oxford University Press.

Arnol'd, V.I., Vogtmann, K., Weinstein, A., 2013. Mathematical methods of classical mechanics. Graduate Texts in Mathematics, 60, 2, illustrated Springer Science & Business Media.

Bai, X.-c., Martin, T.G., Scheres, S.H.W., Dietz, H., 2012. Cryo-EM structure of a 3D DNA-origami object. Proc. Natl. Acad. Sci. 109 (49), 20012–20017. doi:10.1073/pnas.1215713109.
Barkley, M.D., Zimm, B.H., 1979. Theory of twisting and bending of chain macromolecules; analysis of the fluorescence depolarization of DNA. J. Chem. Phys. 70 (6), 2991–3007. doi:10.1063/1.437838.
Bauer, W.R., Lund, R.A., White, J.H., 1993. Twist and writhe of a DNA loop containing intrinsic bends. Proc. Natl. Acad. Sci. 90 (3), 833–837. doi:10.1073/pnas.90.3.833.
Baumann, C.G., Smith, S.B., Bloomfield, V.A., Bustamante, C., 1997. Ionic effects on the elasticity of single DNA molecules. Proc. Natl. Acad. Sci. 94 (12), 6185–6190. doi:10.1073/pnas.94.12.6185.
Bažant, Z.P., 2000. Size effect. Int. J. Solid. Struct. 37 (1), 69–80. doi:10.1016/S0020-7683(99)00077-3.
Bažant, Z.P., Sun, H.-H., 1987. Size effect in diagonal shear failure: influence of aggregate size and stirrups. ACI Mater. J. 84 (4), 259–272.
Benham, C.J., Mielke, S.P., 2005. DNA mechanics. Annual Review of Biomedical Engineering 7 (1), 21–53. doi:10.1146/annurev.bioeng.6.062403.132016. PMID: 16004565
Boles, T.C., White, J.H., Cozzarelli, N.R., 1990. Structure of plectonemically supercoiled DNA. J. Mol. Biol. 213 (4), 931–951. doi:10.1016/s0022-2836(05)80272-4.
Boussinot, F., Monasse, B., 2013. Description of a Molecular Dynamics Simulation System - AA Scale. Technical Report. CEMEF - Centre de Mise en Forme des Matériaux. https://hal-mines-paristech.archives-ouvertes.fr/hal-00773174
Boyd, R.H., 1968. Method for calculation of the conformation of minimum potential-energy and thermodynamic functions of molecules from empirical valence-force potentials — application to the cyclophanes. J. Chem. Phys. 49 (6), 2574–2583. doi:10.1063/1.1670456.
Bryant, Z., Stone, M.D., Gore, J., Smith, S.B., Cozzarelli, N.R., Bustamante, C., 2003. Structural transitions and elasticity from torque measurements on DNA. Nature 424 (6946), 338–341. doi:10.1038/nature01810.
Buehler, M.J., 2006. Nature designs tough collagen: explaining the nanostructure of collagen fibrils. Proceed. Natl. Acad. Sci. 103 (33), 12285–12290. doi:10.1073/pnas.0603216103.
Burrmann, N.J., Moore, J.W., 2013. Development of a web-based, student-centered stereochemistry tutorial. J. Chem. Educ. 90 (12), 1622–1625. doi:10.1021/ed300744s.
Bustamante, C., Bryant, Z., Smith, S.B., 2003. Ten years of tension: single-molecule DNA mechanics. Nature 421 (6921), 423–427. doi:10.1038/nature01405.
Bustamante, C., Smith, S.B., Liphardt, J., Smith, D., 2000. Single-molecule studies of DNA mechanics. Curr. Opin. Struct. Biol. 10 (3), 279–285. doi:10.1016/s0959-440x(00)00085-3.
Case, D.A., 2019. Amber 2019 reference manual (covers Amber18 and AmberTools19). University of California, San Francisco. [Online; accessed 30. April 2019]. http://ambermd.org/doc12/Amber19.pdf
Castro, C.E., Kilchherr, F., Kim, D.-N., Shiao, E.L., Wauer, T., Wortmann, P., Bathe, M., Dietz, H., 2011. A primer to scaffolded DNA origami. Nat. Methods 8 (3), 221–229. doi:10.1038/nmeth.1570.
Champoux, J.J., 2001. DNA topoisomerases: Structure, function, and mechanism. Annual Review of Biochemistry 70 (1), 369–413. doi:10.1146/annurev.biochem.70.1.369. PMID: 11395412
Cluzel, P., Lebrun, A., Heller, C., Lavery, R., Viovy, J.-L., Chatenay, D., Caron, F., 1996. DNA: An extensible molecule. Science 271 (5250), 792–794. doi:10.1126/science.271.5250.792.
Crothers, D.M., Drak, J., Kahn, J.D., Levene, S.D., 1992. [1]DNA Bending, Flexibility, and Helical Repeat by Cyclization Kinetics. In: DNA Structures Part B: Chemical and Electrophoretic Analysis of DNA. In: Methods in Enzymology, Vol. 212. Academic Press, pp. 3–29. doi:10.1016/0076-6879(92)12003-9.
Drugan, W.J., Willis, J.R., 1996. A micromechanics-based nonlocal constitutive equation and estimates of representative volume element size for elastic composites. J. Mech. Phys. Solids 44 (4), 497–524. doi:10.1016/0022-5096(96)00007-5.
Galindo-Murillo, R., Roe, D.R., Cheatham III, T.E., 2015. Convergence and reproducibility in molecular dynamics simulations of the DNA duplex d (GCACGAAC-GAACGAACGC). Biochimica et Biophysica Acta (BBA)-General Subjects 1850 (5), 1041–1058. doi:10.1016/j.bbagen.2014.09.007. Recent developments of molecular dynamics
Garcia-Diaz, M., Kunkel, T.A., 2006. Mechanism of a genetic glissando*: structural biology of indel mutations. Trends Biochem. Sci. 31 (4), 206–214. doi:10.1016/j.tibs.2006.02.004.
Germain, P., 1973. The method of virtual power in continuum mechanics. part 2: microstructure. SIAM J. Appl. Math 25 (3), 556–575. doi:10.1137/0125053.
Gore, J., Bryant, Z., Nöllmann, M., Le, M.U., Cozzarelli, N.R., Bustamante, C., 2006. DNA Overwinds when stretched. Nature 442 (7104), 836–839. doi:10.1038/nature04974.
Grindon, C., Harris, S., Evans, T., Novik, K., Coveney, P., Laughton, C., 2004. Large-scale molecular dynamics simulation of DNA: implementation and validation of the AMBER98 force field in LAMMPS. Philos. Trans. Roy. Soc. Lond. A 362 (1820), 1373–1386. doi:10.1098/rsta.2004.1381.
Gross, P., Laurens, N., Oddershede, L.B., Bockelmann, U., Peterman, E.J.G., Wuite, G.J.L., 2011. Quantifying how DNA stretches, melts and changes twist under tension. Nat. Phys. 7 (9), 731–736. doi:10.1038/nphys2002.
Grüdiac, M., Pierron, F., Avril, S., Toussaint, E., 2006. The virtual fields method for extracting constitutive parameters from full-field measurements: a review. Strain 42 (4), 233–253. doi:10.1111/j.1475-1305.2006.tb01504.x.
Güttler, B., Rienitz, O., Pramann, A., 2019. The Avogadro constant for the definition and realization of the mole. Ann. Phys. 531 (5), 1800292. doi:10.1002/andp.201800292.
Hawkins, G.D., Cramer, C.J., Truhlar, D.G., 1995. Pairwise solute descreening of solute charges from a dielectric medium. Chem. Phys. Lett. 246 (1), 122–129. doi:10.1016/0009-2614(95)01082-K.
Hawkins, G.D., Cramer, C.J., Truhlar, D.G., 1996. Parametrized models of aqueous free energies of solvation based on pairwise descreening of solute atomic charges from a dielectric medium. J. Phys. Chem. 100 (51), 19824–19839. doi:10.1021/jp961710n.
Herrera, J.E., Chaires, J.B., 1989. A premelting conformational transition in poly(dA)-poly(dT) coupled to daunomycin binding. Biochemistry 28 (5), 1993–2000. doi:10.1021/bi00431a006.
Herrero-Galán, E., Fuentes-Perez, M.E., Carrasco, C., Valpuesta, J.M., Carrascosa, J.L., Moreno-Herrero, F., Arias-Gonzalez, J.R., 2013. Mechanical identities of RNA and DNA double helices unveiled at the single-molecule level. J. Am. Chem. Soc. 135 (1), 122–131. doi:10.1021/ja3054755.
Hill, R., 1963. Elastic properties of reinforced solids: some theoretical principles. J. Mech. Phys. Solid. 11 (5), 357–372. doi:10.1016/0022-5096(63)90036-x.
Hill, R., 1965. Continuum micro-mechanics of elastoplastic polycrystals. J. Mech. Phys. Solid. 13 (2), 89–101. doi:10.1016/0022-5096(65)90023-2.
Höller, R., Aminbaghai, M., Eberhardsteiner, L., Eberhardsteiner, J., Blab, R., Pichler, B.L.A., Hellmich, C., 2019. Rigorous amendment of Vlasov's theory for thin elastic plates on elastic Winkler foundations, based on the principle of virtual power. Eur. J. Mech. A. Solids 73, 449–482. doi:10.1016/j.euromechsol.2018.07.013.
Ilse, S.E., 2016. Classical atomistic force fields for single-and double-stranded DNA. Institute for Computational Physics-University of Stuttgart. [Online; accessed 08. Mai 2018]. https://www.icp.uni-stuttgart.de/~icp/mediawiki/images/archive/f/f9/20160529114111!Handout_ilse_HS_SS16.pdf.
Ivani, I., 2016. Parmbsc1: Parameterization and Validation of a new State-of-the-art Force Field for DNA Simulations. Universitat de Barcelona, Barcelona, Spain. [Online; accessed 12. October 2017]. http://hdl.handle.net/2445/110725.
Ivani, I., Dans, P.D., Noy, A., Pérez, A., Faustino, I., Hospital, A., Walther, J., Andrio, P., Goñi, R., Balaceanu, A., Portella, G., Battistini, F., Gelpi, J.L., Gonzalez, C., Vendruscolo, M., Laughton, C.A., Harris, S.A., Case, D.A., Orozco, M., 2016. Parmbsc1: a refined force-field for DNA simulations. Nat. Methods 13 (1), 55–58. doi:10.1038/nmeth.3658.
Keten, S., Xu, Z., Ihle, B., Buehler, M.J., 2010. Nanoconfinement controls stiffness, strength and mechanical toughness of β-sheet crystals in silk. Nat. Mater. 9 (4), 359–367. doi:10.1038/nmat2704.

Kim, Y.-J., Kim, D.-N., 2016. Structural basis for elastic mechanical properties of the DNA double helix. PLoS ONE 11 (4), e0153228. doi:10.1371/journal.pone.0153228.
von Klitzing, K., 2019. Essay: quantum hall effect and the new international system of units. Phys. Rev. Lett. 122 (20), 200001. doi:10.1103/PhysRevLett.122.200001.
Kosikov, K.M., Gorin, A.A., Zhurkin, V.B., Olson, W.K., 1999. DNA Stretching and compression: large-scale simulations of double helical structures. J. Mol. Biol. 289 (5), 1301–1326. doi:10.1006/jmbi.1999.2798.
Kothari, P., Johnson, C., Sandone, C., Iglesias, P.A., Robinson, D.N., 2019. How the mechanobiome drives cell behavior, viewed through the lens of control theory. J. Cell. Sci. 132 (17), jcs234476. doi:10.1242/jcs.234476.
Kuttke, P., Kurfürst, A., Scheiner, S., Hellmich, C., 2019. Sequential 1D/2D finite element analyses of tramway rails under bending and restrained torsion, based on the principle of virtual power. Mech. Adv. Mater. Struct. 0 (0), 1–23. doi:10.1080/15376494.2019.1647317.
Königsberger, M., Pichler, B.L.A., Hellmich, C., 2020. Multiscale poro-elasticity of densifying calcium-silicate hydrates in cement paste: an experimentally validated continuum micromechanics approach. Int. J. Eng. Sci. 147, 103196. doi:10.1016/j.ijengsci.2019.103196.
Lavery, R., Lebrun, A., Allemand, J.-F., Bensimon, D., Croquette, V., 2002. Structure and mechanics of single biomolecules: experiment and simulation. J. Phys. 14 (14), R383–R414. doi:10.1088/0953-8984/14/14/202.
Lavery, R., Zakrzewska, K., Beveridge, D., Bishop, T.C., Case, D.A., Cheatham III, T.E., Dixit, S., Jayaram, B., Lankas, F., Laughton, C., Maddocks, J.H., Michon, A., Osman, R., Orozco, M., Perez, A., Singh, T., Spackova, N., Sponer, J., 2010. A systematic molecular dynamics study of nearest-neighbor effects on base pair and base pair step conformations and fluctuations in B-DNA. Nucleic Acids Res. 38 (1), 299–313. doi:10.1093/nar/gkp834.
Lengvarsky, P., Bocko, J., 2015. Prediction of Young's modulus of graphene sheets by the finite element method. Am. J. Mech. Eng. 3 (6), 225–229. doi:10.12691/ajme-3-6-14.
Lionnet, T., Joubaud, S., Lavery, R., Bensimon, D., Croquette, V., 2006. Wringing out DNA. Phys. Rev. Lett. 96 (17), 178102. doi:10.1103/PhysRevLett.96.178102.
Lu, X., Olson, W.K., 2003. 3DNA: A software package for the analysis, rebuilding and visualization of three-dimensional nucleic acid structures. Nucleic Acids Res. 31 (17), 5108–5121. doi:10.1093/nar/gkg680.
Macke, T.J., Case, D.A., 1997. Modeling Unusual Nucleic Acid Structures. In: Molecular Modeling of Nucleic Acids; ACS Symposium Series, Vol. 682. American Chemical Society, pp. 379–393. doi:10.1021/bk-1998-0682.ch024.
Mathew-Fenn, R.S., Das, R., Harbury, P.A.B., 2008. Remeasuring the double helix. Science 322 (5900), 446–449. doi:10.1126/science.1158881.
Modeling, Molecular and Group, B., 2016. ParmBSC1 forcefield nucleotide MD simulations database. [Online; accessed 11. October 2017]. http://mmb.pcb.ub.es/www/ParmBSC1.
Monasse, B., Boussinot, F., 2014. Determination of forces from a potential in molecular dynamics. arXiv e-prints. https://arxiv.org/abs/1401.1181.
Moroz, J.D., Nelson, P., 1997. Torsional directed walks, entropic elasticity, and DNA twist stiffness. Proceed. Natl. Acad. Sci. 94 (26), 14418–14422. doi:10.1073/pnas.94.26.14418.
Naserian-Nik, A.M., Tahani, M., Karttunen, M., 2013. Pulling of double-stranded DNA by atomic force microscopy: a simulation in atomistic details. RSC Adv. 3 (26), 10516–10528. doi:10.1039/C3RA23213A.
Olson, W.K., Marky, N.L., Jernigan, R.L., Zhurkin, V.B., 1993. Influence of fluctuations on DNA curvature: a comparison of flexible and static wedge models of intrinsically bent DNA. J. Mol. Biol. 232 (2), 530–554. doi:10.1006/jmbi.1993.1409.
Orozco, M., Noy, A., Pérez, A., 2008. Recent advances in the study of nucleic acid flexibility by molecular dynamics. Curr. Opin. Struct. Biol. 18 (2), 185–193. doi:10.1016/j.sbi.2008.01.005.
Ouldridge, T.E., Louis, A.A., Doye, J.P.K., 2011. Structural, mechanical, and thermodynamic properties of a coarse-grained DNA model. J. Chem. Phys. 134 (8), 85101. doi:10.1063/1.3552946.
Palma, M., Scheller, C.P., Maradan, D., Feshchenko, A.V., Meschke, M., Zumbühl, D.M., 2017. On-and-off chip cooling of a coulomb blockade thermometer down to 2.8 mk. Appl. Phys. Lett. 111 (25), 253105. doi:10.1063/1.5002565.
Pearlman, D.A., Case, D.A., Caldwell, J.W., Ross, W.S., Cheatham III, T.E., DeBolt, S., Ferguson, D., Seibel, G., Kollman, P.A., 1995. AMBER, A package of computer programs for applying molecular mechanics, normal mode analysis, molecular dynamics and free energy calculations to simulate the structural and energetic properties of molecules. Comput. Phys. Commun. 91 (1–3), 1–41. doi:10.1016/0010-4655(95)00041-D.
Pérez, A., Marchán, I., Svozil, D., Sponer, J., Cheatham III, T.E., Laughton, C.A., Orozco, M., 2007. Refinement of the AMBER force field for nucleic acids: improving the description of α/γ conformers. Biophys. J. 92 (11), 3817–3829. doi:10.1529/biophysj.106.097782.
Peters, J.P., Yelgaonkar, S.P., Srivatsan, S.G., Tor, Y., Maher, L.J., 2013. Mechanical properties of DNA-like polymers. Nucleic Acids Res. 41 (22), 10593–10604. doi:10.1093/nar/gkt808.
Podgornik, R., Hansen, P.L., Parsegian, V.A., 2000. Elastic moduli renormalization in self-interacting stretchable polyelectrolytes. J. Chem. Phys. 113 (20), 9343–9350. doi:10.1063/1.1319380.
Poli, M., Gatta, L.B., Dominici, R., Lovati, C., Mariani, C., Albertini, A., Finazzi, D., 2005. DNA Sequence variations in the prolyl isomerase pin1 gene and alzheimer's disease. Neurosci. Lett. 389 (2), 66–70. doi:10.1016/j.neulet.2005.07.027.
Portella, G., Battistini, F., Orozco, M., 2013. Understanding the connection between epigenetic DNA methylation and nucleosome positioning from computer simulations. PLoS Comput. Biol. 9 (11), e1003354. doi:10.1371/journal.pcbi.1003354.
Rothemund, P.W.K., 2006. Folding DNA to create nanoscale shapes and patterns. Nature 440 (7082), 297–302. doi:10.1038/nature04586.
Salenccon, J., Lyle, S., 2001. Handbook of Continuum Mechanics: General Concepts Thermoelasticity, 1 Springer-Verlag Berlin Heidelberg doi:10.1007/978-3-642-56542-7. Original French edition published by Editions de l'Ecole polytechnique, Palaiseau, France, 2000
Sengupta, P.P., Tajik, A.J., Chandrasekaran, K., Khandheria, B.K., 2008. Twist mechanics of the left ventricle. JACC: Cardiovascular Imaging 1 (3), 366–376. doi:10.1016/j.jcmg.2008.02.006.
Smith, S.B., Finzi, L., Bustamante, C., 1992. Direct mechanical measurements of the elasticity of single DNA molecules by using magnetic beads. Science 258 (5085), 1122–1126. doi:10.1126/science.1439819.
Šponer, J., Jurečka, P., Marchan, I., Luque, F.J., Orozco, M., Hobza, P., 2006. Nature of base stacking: reference quantum-chemical stacking energies in ten unique B-DNA base-pair steps Chem.-Eur. J. 12, 2854–2865 doi:10.1002/chem.200501239.
Srivastava, P.K., 1997. Mechanics. New Age International Pub. (P) Limited.
Strauss, F., Gaillard, C., Prunell, A., 1981. Helical periodicity of DNA, poly(dA) · poly(dT) and poly(dA-dT) · poly(dA-dT) in solution.. Eur. J. Biochem. 118 (2), 215–222. doi:10.1111/j.1432-1033.1981.tb06389.x.
Swails, J., Hernandez, C., Mobley, D. L., Nguyen, H., Wang, L.-P., Janowski, P., 2014. Parmed. [Online; accessed 02. March 2020]. https://github.com/ParmEd/ParmEd/blob/master/parmed/tools/changeradii.py.
Swails, J.M., 2013. Free energy simulations of complex biological systems at constant pH. University of Florida. [Online; accessed 24. July 2018]. http://ufdcimages.uflib.ufl.edu/UF/E0/04/57/41/00001/SWAILS_J.pdf
Swails, J. M., Roitberg, A. E., Amber, 2013. prmtop file of Amber. [Online; accessed 01. January 2018]. http://ambermd.org/prmtop.pdf.
The MathWorks, 2019. Matlab R2019a. [Online; accessed 28. Febuary 2020]. https://de.mathworks.com/products/new_products/release2019a.html.
Touratier, M., 1991. An efficient standard plate theory. Int. J. Eng. Sci. 29 (8), 901–916. doi:10.1016/0020-7225(91)90165-Y.
Tsui, V., Case, D.A., 2001. Theory and applications of the generalized born solvation model in macromolecular simulations. Biopolymers 56 (4), 275–291. doi:10.1002/1097-0282(2000)56:4<275::AID-BIP10024>3.0.CO;2-E.
Uberuaga, B.P., Anghel, M., Voter, A.F., 2004. Synchronization of trajectories in canonical molecular-dynamics simulations: observation, explanation, and exploitation. J. Chem. Phys. 120 (14), 6363–6374. doi:10.1063/1.1667473.
Wang, M.D., Yin, H., Landick, R., Gelles, J., Block, S.M., 1997. Stretching DNA with optical tweezers. Biophysical Journal 72 (3), 1335–1346. doi:10.1016/S0006-3495(97)78780-0. 9138579[pmid].

Wood, B., Bettin, H., 2019. The planck constant for the definition and realization of the kilogram. Ann. Phys. 531 (5), 1800308. doi:10.1002/andp.201800308.
Wu, Y.-Y., Bao, L., Zhang, X., Tan, Z.-J., 2015. Flexibility of short DNA helices with finite-length effect: from base pairs to tens of base pairs. J. Chem. Phys. 142 (12), 125103. doi:10.1063/1.4915539.
Yoo, K.-H., Ha, D.H., Lee, J.-O., Park, J.W., Kim, J., Kim, J.J., Lee, H.-Y., Kawai, T., Choi, H.Y., 2001. Electrical conduction through poly(dA)-poly(dT) and poly(dG)-poly(dC) DNA molecules. Phys. Rev. Lett. 87 (19), 198102. doi:10.1103/PhysRevLett.87.198102.
Zaoui, A., 2002. Continuum micromechanics: survey. J. Eng. Mech. 128 (8), 808–816. doi:10.1061/(ASCE)0733-9399(2002)128:8(808).